

2023 senesi İTÜ'ye iyi gelmedi. Önce Yusuf, arkadan Aral gitti ve her ikisi de İTÜ'nün akademik performansında büyük iki delik bıraktılar. Yusuf benim iyi bir dostum, bazen da dert ortağımdı. Derdimiz ise Türkiye'nin bilim dünyasındaki yeri idi. Yusuf üstün başarılı bir kimyacıydı ve en son konuştuğumuzda ona Nobel getirebilecek projelerini anlatmıştı. Ben de ona eğer Nobel alırsa, İTÜ kampüsünün ortasına çıkıp zevkten göbek atacağını söylemiştim. Ne yazık ki ölümü buna izin vermedi.

Yusuf'la bilimsel ilgilerimiz birbirlerinden epey farklı olduğu için bir araya geldiğimizde oradan buradan sohbet ederdik, Türkiye'nin bilimdeki geriliğinden de dem vurup üzüntülerimizi paylaşırdık. Ama Yusuf asla kötümser değildi. Müthiş zekâsı ve hazırcevaplığı, nüktedanlığına ayrı bir lezzet katardı. Ben Yusuf'u hiç asık yüzlü görmemişim. Ama ölümü hepimizin yüzünü astı, en azından ben hâlâ yüzümü eski haline getiremiyorum. Onun esprilerini, hınzır sataşmalarını düşünüyorum gülebilmek için, ama onları yapan ortada olmayınca yüzüm eski haline gelmeyi reddediyor. Şimdi Yusuf'un arkada bıraktıklarına düşen en önemli görev onun başlattığı ivmeyi hızlandırarak sürdürmek ve onun almasını hepimizin çok istediği kimya Nobel ödülünü üniversitemize getirmek.

O zaman da İTÜ belki dünya çapında arzu edilen bir "Yusuf Yağcı Kimya Madalyasını" hayata geçirir, bizden sonraki nesiller Yusuf'un o her zaman gülümseyen, dost yüzünü bir altın yüzeyde görüp heyecanlarına heyecan katabilirler.

Yusuf öldü. Ama onun eserinin, onun azîz hâtırasının ilelebet yaşamasını temin etmek artık arkada bıraktığı bizlerin borcudur. Nur içinde yat azîz arkadaşım. Senin saçtığın ışıklar hepimizin sanki daha da pırıltılı görülmemizi sağlıyor bu çeyrek bin yıllık üniversitemizde. İnan, sen kalbimizde her zaman var olacaksın, anılarında İTÜ'ye nur yağdırmaya devam edeceksin.

Hyaluronic Acid-Enriched Pectin-Based Hydrogel Films for Wound Healing

Ö. Zeynep Güner Yılmaz¹, F. Seniha Güner^{1,2}

¹ Istanbul Technical University, Department of Chemical Engineering, Maslak 34469 Istanbul, Turkey

² Sabancı University Nanotechnology Research and Application Center (SUNUM), Tuzla 34956 Istanbul, Turkey

Corresponding Author: F. Seniha Güner, guners@itu.edu.tr; seniha.guner@sabanciuniv.edu

Abstract: Wound healing research is always looking for approaches to improve patient care. Advanced wound dressings are critical in this process. In this context, the article focuses on the comprehensive examination of the potential of hyaluronic acid-enriched pectin-based hydrogel films to advance wound healing. For comparative analysis, two formulations were prepared: a pectin matrix and a film containing fifty percent hyaluronic acid and pectin. Both formulations were cross-linked using calcium ions. The hydrogels underwent thorough characterization, including Fourier-transform infrared spectroscopy analysis for chemical composition, differential scanning calorimetry for thermal properties determination, and scanning electron microscope imaging for morphological examination of cross-sections. We thoroughly examine their fluid-handling capacities, dehydration rates, and water vapor permeability through meticulous inspection. These characteristics have a significant impact on elasticity, moisture retention, and overall effectiveness throughout the healing process. To demonstrate the transformative potential of HA-enriched pectin-based hydrogel films, we compare their properties to those of pectin hydrogel and a commercial alginate-based wound dressing. As a result, the investigation revealed a notable enhancement in the transparency of the wound dressing, a crucial factor for facilitating continuous monitoring of the wound site without necessitating frequent removal of the dressing. The improvement in water vapor permeability suggests an optimized moisture balance, fostering an environment conducive to efficient wound healing. Moreover, the smoother film contributes to the overall comfort for patients and potentially minimizes skin irritation and discomfort during prolonged wear. The innovative features identified in this study collectively point towards the prospect of these hydrogel films not only as effective wound dressings but also as a step forward in addressing the practical aspects of patient comfort and convenience.

Keywords: Pectin, Hyaluronic acid, Hydrogel, Wound treatment

Yara İyileşmesi için Hiyalüronik Asitle Zenginleştirilmiş Pektin Temelli Hidrojel Filmler

Özet: Yara iyileşmesi araştırmaları her zaman hasta bakımını iyileştirecek yaklaşımlar arar. Gelişmiş yara örtüleri bu süreçte kritik öneme sahiptir. Bu bağlamda makale, hiyalüronik asit ile zenginleştirilmiş pektin bazlı hidrojel filmlerin yara iyileşmesi sürecini hızlandırma potansiyelinin kapsamlı bir şekilde incelenmesine odaklanmaktadır. Karşılaştırmalı analiz için iki formülasyon hazırlanmıştır: pektin matrisi ve yüzde elli hiyalüronik asit ve pektin içeren bir film. Her iki formülasyon da kalsiyum iyonları kullanılarak çapraz bağlanmıştır. Hidrojeller, kimyasal bileşim için Fourier dönüşümü kızılötesi spektroskopisi analizi, termal özelliklerin belirlenmesi için diferansiyel taramalı kalorimetre ve kesitlerin morfolojik incelemesi için taramalı elektron mikroskobu görüntüleme dahil olmak üzere kapsamlı bir karakterizasyona tabi tutulmuştur. Ayrıca sıvı taşıma kapasitelerini, dehidrasyon oranlarını ve su buharı geçirgenliği incelenmiştir. Bu özellikler iyileşme süreci boyunca elastikiyeti, nem tutmayı ve genel etkinliği önemli ölçüde etkiler. Hiyalüronik asit ile zenginleştirilmiş pektin bazlı hidrojel filmlerin potansiyelini göstermek için, pektin hidrojelinde ticari aljinat bazlı yara örtüsüyle karşılaştırılmıştır. Sonuç olarak araştırma, yara örtüsünün şeffaflığında gözle görülür bir artış olduğunu ortaya çıkarmıştır; bu, yara örtüsünün sık sık değiştirilmesini gerektirmeden yara bölgesinin sürekli takibini kolaylaştırmak için çok önemli bir faktördür. Su buharı geçirgenliğindeki iyileşme, optimize edilmiş bir nem dengesine işaret ederek etkili yara iyileşmesine olanak sağlayan bir ortam sağlamaktadır. Dahası, katkı ile daha pürüzsüz olan film hastalar için genel konfora katkıda bulunur ve uzun süreli kullanım sırasında cilt tahrişini ve rahatsızlığını potansiyel olarak en aza indirir. Bu çalışmada belirlenen özellikler, sadece etkili bir yara bandı olmanın ötesinde, aynı zamanda hasta konforu ve kullanım kolaylığına yönelik pratik gelişmeleri ele alarak bir adım öteye taşıyabilir.

Anahtar Kelimeler: Pektin, Hiyalüronik asit, Hidrojel, Yara tedavisi

RESEARCH PAPER

Citation: Zeynep Güner Yılmaz, F. Seniha Güner, (2024), Hyaluronic Acid-Enriched Pectin-Based Hydrogel Films for Wound Healing, ITU ARI Bulletin of the Istanbul Technical University 55,(2) 15–22.

Submission Date: 13 November 2023

Online Acceptance: 14 January 2024

Online Publishing: 15 January 2024

1. Introduction

Wound healing represents a fundamental and ever-evolving piece of medical research and healthcare, continually striving to enhance the recovery process and elevate patient care. A pivotal component in this domain is the development of advanced wound dressings, which play a crucial role in shaping the trajectory of wound healing. In the existing literature, extensive research has been carried out on hydrogel-based wound dressings, utilizing materials that encompass both synthetic polymers and biopolymers (Chauhan et al., 2022; Divyashri et al., 2022). Among the diverse array of hydrogel wound dressing materials, pectin, a natural polysaccharide, has risen to prominence for its remarkable properties. Pectin-based wound dressings have garnered considerable attention due to their inherent biocompatibility, moisture-retention characteristics, and flexibility. Within the spectrum of wound care, pectin-based hydrogel wound dressings offer a versatile platform, welcoming various additive materials to enhance their performance (Güner et al., 2021; Kumar et al., 2013; S. Bin Wang et al., 2004). The incorporation of diverse additives has led to the development of innovative wound dressings that are tailored to specific clinical needs.

One of the notable additives in this context is hyaluronic acid (HA), which has emerged as a frontrunner for its distinctive properties and compatibility with wound dressing materials (Mero & Campisi, 2014). HA, a naturally occurring biopolymer, is renowned for its ability to bind with water molecules, thereby maintaining an optimal moisture balance—a crucial factor in wound healing (Liao et al., 2018; Price et al., 2005). Its unique molecular structure makes it an ideal candidate for integration into wound dressings, where the preservation of a moist wound environment is imperative. Numerous studies conducted over the years have consistently underscored the advantages of HA-enriched wound dressings such as chitosan, gelatin, alginate, pectin, or a combination of two or more (Bozer et al., 2023; Tarusha et al., 2018; Yang et al., 2019; Zhou et al., 2014). These findings underscore HA's potential as a key component in innovative wound dressings tailored to meet diverse clinical needs.

In this context, this article focuses on the comprehensive investigation of HA-enriched pectin-based hydrogel films and their potential to advance wound healing. In contrast to the commonly used inter-chain cross-linking method in the literature, we adopted a simpler film preparation process that did not involve cross-linking the chains. Through a rigorous examination of their mechanical attributes, fluid-handling capabilities, dehydration rates, and water vapor permeability, this study seeks to evaluate their suitability for wound healing applications. This study embarks on a comprehensive exploration and evaluation of HA-enriched pectin hydrogel films as prospective wound dressings. The inquiry encompasses an array of critical parameters, spanning mechanical attributes, fluid-handling capacity, dehydration kinetics, and water vapor permeability. The study covers a wide range of critical factors, all of which have a significant impact on the pliability and capacity of wound dressings to maintain an optimal moisture environment during the healing process.

2. Materials and Methods

2.1. Chemicals

41% amidated low-methoxy citrus pectin provided by Herbstreith & Fox KG (Neuenbürg, Germany) was used as the polymer matrix. Hyaluronic acid (HA) with a molecular weight of 3000-5000 was provided from HD Uluslararası Ticaret ve Ambalaj Sanayi Ltd. Sti. (Kocaeli, Turkey). In addition, glycerol (Labkim, Istanbul, Turkey) was used as a plasticizer. The calcium chloride used as a crosslinker was in analytical purity. The structure of pectin and HA are given in Figure 1.

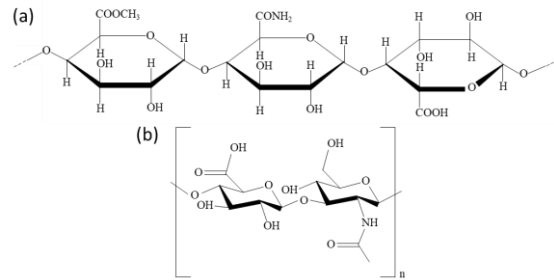


Figure 1. Chemical structure of (a) low-methoxy amidated pectin, (b) hyaluronic acid.

2.2. Preparation of hydrogels

Hyaluronic acid-loaded hydrogels were prepared with a similar method used in our previous studies (Güner et al., 2018, 2021). The experimental procedure to prepare hydrogels is shown in Figure 2. In brief, pectin and HA were dissolved in ultrapure water at 1% w.w⁻¹, then 15 mL of each solution was mixed. Then glycerol solution (5% w.w⁻¹) was added and mechanically stirred at 150 rpm for 2 h. After preparing a homogeneous mixture, %0.7 CaCl₂ solution (10 mL) is added to a Petri plate to form a crosslinked hydrogel (Pe-HA). The hydrogel is left to dry in an orbital shaker at 25°C. As a comparison, a pectin hydrogel (Pe) is prepared with pectin, glycerol, and CaCl₂ without the hyaluronic acid addition.

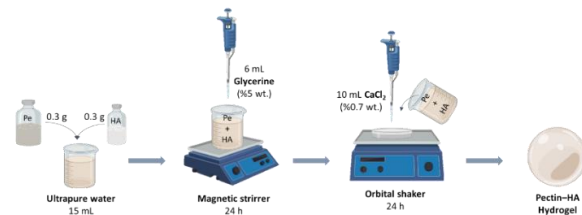


Figure 2. Preparation of hyaluronic acid-pectin hydrogel.

2.3. Characterization of hydrogels

Fourier-transform infrared (FT-IR) spectroscopy analysis was performed on a Perkin Elmer Spectrum 100 spectrometer model between 650 and 4000 cm⁻¹ using the ATR mode.

Thermal properties of the hydrogels were determined with a Perkin Elmer 4000 differential scanning calorimeter (DSC) under a nitrogen atmosphere. Analyzes were performed between -50 and 300°C with a scan rate of 10°C/min.

Scanning electron microscope (SEM) images of cross-sections of hydrogel samples were produced for morphological examination using Jeol JSM-6390LV. Samples were fractured in liquid nitrogen and then coated with platinum using a sputter coater.

2.4. Swelling behavior of hydrogels

The evaluation of the hydrogel films' swelling behavior involved a systematic procedure. Initially, dried samples were cut to a 10 mm diameter each, and their weights were recorded as W_1 . Subsequently, these samples were immersed in a 10 mL buffer solution, and data points were collected at different time intervals. After removal from the buffer solution, excess water was efficiently absorbed using filter paper, followed by weighing the samples denoted as W_2 . The swelling ratio of the hydrogels was then accurately calculated utilizing Equation 1.

$$\text{Swelling} = \frac{W_2 - W_1}{W_1} \quad (1)$$

2.5. Wound dressing properties of hydrogels

To obtain information about the behavior of the prepared hydrogels in the wound environment, the wound dressing properties were examined under in vitro conditions.

The Shore A hardness of the samples was determined with a durometer according to ASTM D2240. The Shore A hardness scale measures the hardness of flexible rubbers and semi-rigid plastics (American Society for Testing and Materials, 2015).

The flexibility of the samples was measured according to the ASTM-D-522 standard with an Erichsen Model 266S bending tester with 14 stainless steel cylinders from 2 to 32 mm in diameter (Methods, 2001). The test determines the smallest cylinder diameter at which a sample does not show cracking after bending.

BS EN 13726-1:2002 standard was used to determine the fluid handling of the samples (Updated et al., 2016). Briefly, a hydrogel film was cut into a 5 cm × 5 cm square, weighed (W_{D1}), and placed in a Petri dish. Then, a salt solution prepared by adding 2.298 g NaCl and 0.368 g $\text{CaCl}_2 \cdot 2\text{H}_2\text{O}$ in 1 L of deionized water was heated to $37 \pm 1^\circ\text{C}$ and added to the Petri dish at a ratio of 1:40 (wt.volume⁻¹). The Petri dish was placed in the incubator at $37 \pm 1^\circ\text{C}$ for 30 minutes and then removed from the incubator. The hydrogel was held in one corner using tweezers and allowed to drip off excess water for 30 seconds. The hydrogel was reweighed to calculate the mass of the solution absorbed by the hydrogel (W_w). Equation 2 was used to calculate the fluid handling.

$$\text{Fluid handling} = \frac{W_w - W_{D1}}{W_{D1}} \quad (2)$$

To determine the in vitro dehydration rate, the sample (5 cm × 5 cm) was first dried at $37 \pm 1^\circ\text{C}$ for 24 hours. Then, it was kept in deionized water at $37 \pm 1^\circ\text{C}$, taken out of the water after 30 minutes, held from one corner with tweezers for 30 seconds to remove excess water, and weighed again (W_w). The sample was then dried again at $37 \pm 1^\circ\text{C}$ for 24 hours ($T = 1440$ min) and weighed (W_{D2}). The dehydration rate was calculated according to Equation 3.

$$\text{Dehydration Rate (g.min}^{-1}\text{)} = \frac{W_w - W_{D2}}{T} \quad (3)$$

The water vapor permeability of the synthesized samples was determined according to ASTM E96-00 standards (Conshohocken, 1996). For this purpose, the sample was cut with a round mold with an area (a) of 3.14 cm², masked with aluminum foil, and glued to the mouth of sample containers filled with silica. The sample container was weighed (W_1) and placed in a desiccator containing saturated NaCl solution. It was reweighed (W_2) at regular intervals from the beginning on a daily basis, and water vapor permeability was calculated according to Equation 4. Simultaneously, the corresponding day of each measurement from the start was recorded (T).

$$\text{Water Vapor Permeability (g.m}^{-2}\text{day}^{-1}\text{)} = \frac{W_2 - W_1}{a \cdot W_1 \cdot T} \quad (4)$$

The average mass per unit area (g.m⁻²) of hydrogels was determined according to the BS EN 12127:1997 standard (BS EN 12127:1997). The dry sample was cut into 5 cm × 5 cm dimensions, weighed and the resulting value was divided by area.

The water contact angle was measured using a Biolink Scientific Attension Theta Flex goniometer at room temperature by placing 4 μL of distilled water on the hydrogel surface using the sessile drop method.

Additionally, the change in the transparency of the film by adding HA to the matrix was examined. For this purpose, the transparency test was carried out using a UV-Vis spectrophotometer (LAMBDA 1050) as in the literature (Andriotis et al., 2020; Farahnaky et al., 2018; Martucci & Ruseckaite, 2010). The films were cut into a rectangular shape and placed on the outside of the spectrophotometer cell, and measurements were made at 550 nm, which is the wavelength at which the human eye perceives colors. transparency was calculated using Equation 5, where A is the absorbance.

$$\text{Transparency} = 10^{(2-A)} \quad (5)$$

The dispersion properties of wound dressings are an indicator of their mechanical strength when interacting with fluid during wound healing. Therefore, the dispersion property of the sample was measured according to the BS EN 13726-2:2001 standard (Updated et al., 2016). A 5 cm × 5 cm sample was cut from the hydrogel and placed in a 250 mL of the prepared salt solution (NaCl and $\text{CaCl}_2 \cdot 2\text{H}_2\text{O}$) was added and rotated gently for 60 seconds so as not to create a vortex. The integrity of the hydrogel was then visually categorized as “dispersible” or “non-dispersible”.

3. Results and Discussion

In this section, we discuss the key findings from our in vitro characterization studies on the prepared hydrogels and their wound dressing properties. The results shed light on the potential of these hydrogels for wound healing applications.

more comfortable environment when placed on the wound, which is a crucial feature for wound healing applications.

3.1. Characterization of Hydrogel Structure

The FT-IR spectra of the hydrogels are presented in Figure 3. Spectrum analysis revealed the incorporation of HA into Pe film, as evidenced by the characteristic peaks of HA (de Oliveira et al., 2017; Grkovic et al., 2015) and Pe film in Pe-HA film, indicating a high degree of compatibility between the two components. Specifically, the C-O-C (1094 cm^{-1}), sp³ C-H (1420 cm^{-1}), and N-H (1619 cm^{-1}) peaks are observed in HA, Pe, and Pe-HA. In conjunction with these, the O-H peak ($3200\text{--}2900\text{ cm}^{-1}$), primarily arising from the carboxylic acid in Pe, and the C-H aliphatic stretching band (2900 and 2800 cm^{-1}) are specific to Pe and Pe-HA.

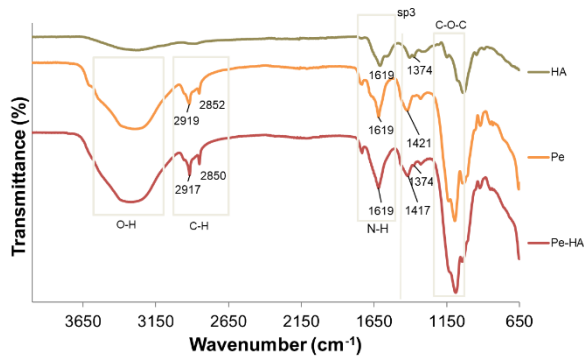


Figure 3. FT-IR Spectra of HA, Pe, and HA-Pe.

DSC analysis provides insights into the thermal characteristics of HA and Pe-HA hydrogels. (Figure 4) The glass transition temperatures (T_g) of Pe, and HA-Pe were found to be 40.1°C , and 38.6°C , respectively. Additionally, the significant sharp exothermic peak suggested that a thermal degradation occurred at around 226°C for HA and 240°C for Pe-HA (Kafedjiiski et al., 2007). Modification of HA by pectin caused the exothermic peak to shift to higher decomposition temperatures compared to HA. The difference is about 14°C . On the other hand, an endothermic peak was observed in the DSC curve of pectin indicating the presence of water, hydrogen bonding among the galacturonic acid units, and conformational changes of the galacturonan ring (Taufiq & Saifullah, 2019; W. Wang et al., 2016).

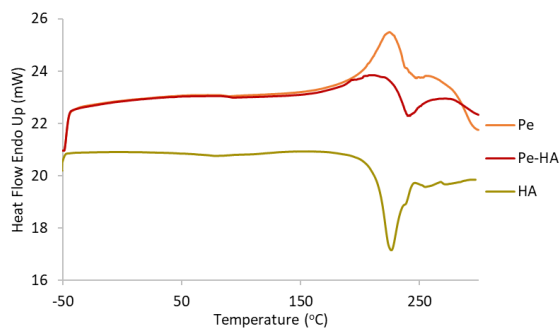


Figure 4. DSC curves of Pe, HA, and Pe-HA

For morphological analysis, images of cross-sections of hydrogel samples were obtained using SEM. According to SEM images given in Figure 5, it was determined that the pectin film structure became smoother with the addition of HA. This is an indication that HA-Pe hydrogels will create a

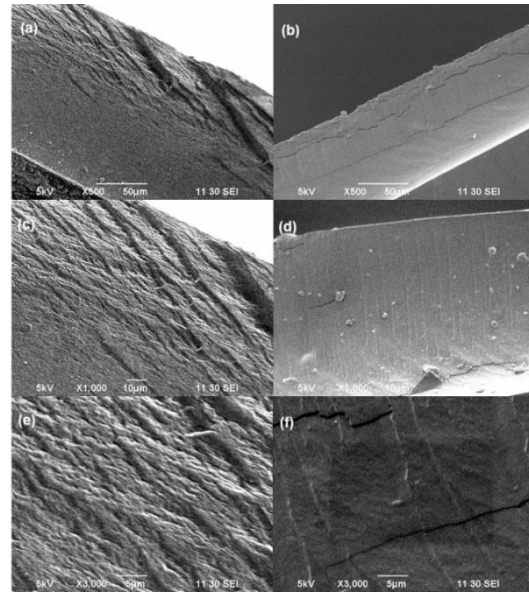


Figure 5. SEM images at different magnifications: (a, c, and d) Pe and (b, d, and f) HA-Pe.

3.2. Wound Dressing Properties of Hydrogels

The pH of a wound environment plays a crucial role in the healing process. It is well accepted that as a wound heals, the pH of the wound milieu falls. Our study investigated the swelling behavior of Pe-HA hydrogels at pH levels of 4.6, 6.4, and 8.0 within the initial 24 hours. The data shown in Figure 6 show that the swelling of both samples increases in time as expected. Furthermore, the addition of HA improves the hydrogels' ability to retain water at pH 4.6 and pH 6.4. The ionization of -COOH groups in pectin (Gałkowska et al., 2003) and hyaluronic acid within the release medium promotes polymer swelling, driven by osmotic pressure until an equilibrium is reached. Given the gradual decrease in wound pH during healing, these findings highlight the suitability of HA-Pe hydrogels for maintaining an optimal moist wound environment.

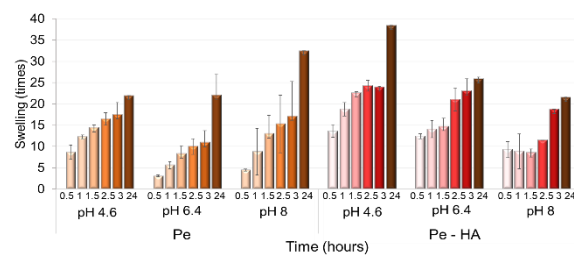


Figure 6. Swelling behavior of Pe and Pe-HA films at pH 4.6, 6.4, and 8.

Due to the hyaluronic acid addition, the pectin hydrogel's contact angle increased by 30 degrees (Figure 7), indicating a considerable increase in surface hydrophobicity. Pectin hydrogels, when enhanced with hyaluronic acid, exhibit a significant increase in contact angle, indicating improved surface hydrophobicity. In the context of wound dressings, this heightened hydrophobicity can help to repel excess

moisture, maintaining the vital moist environment required for effective wound healing.

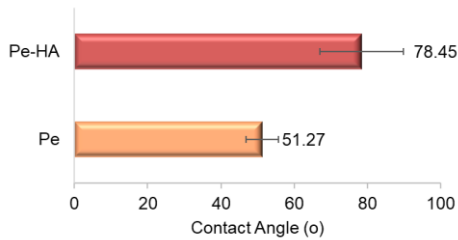


Figure 7. Water contact angle measurements of Pe and Pe-HA.

In the context of wound dressings, some properties of the hydrogels are given in Table 3. The Shore A hardness values may be an indication of protecting the wound against external physical forces. The Shore A value for Pe-HA is approximately twice that of Pe. A higher Shore A value, such as in Pe-HA, indicates greater rigidity, making it suitable for wound dressings that require structural support and stability, which could be essential for wounds needing protection.

Conversely, the lower Shore A value of PE suggests increased flexibility, which can be advantageous in dressings designed for areas where adaptability and comfort are prioritized, like sensitive or curved body contours. This flexibility may enhance patient comfort during the healing process. Therefore, the choice between Pe-HA and Pe for wound dressings should depend on the specific requirements of the wound and the level of support and comfort needed.

The results of various experiments demonstrating the performance of wound dressings are presented in Table 3. In this context, a comparison is made with Kaltostat, a commercially available alginate-based wound dressing widely used for wound care. There is a wide variety of wound dressing matrices available. Due to Kaltostat being alginate-based, our film, which is pectin-based and shares a mirrored chemical structure in terms of carbohydrate composition, is selected for comparison in this study. This choice is made to provide a suitable basis for comparison due to the chemical similarities between the two materials.

Table 3. Wound dressing performance of hydrogels.

Sample Code	Shore A Hardness	Flexibility ^b (mm)	Fluid Handling (g.g ⁻¹)	Dehydration Rate x 103 (g.min ⁻¹)	Mass per Unit Area (g.m ⁻²)	Transparency	Dispersion
Pe	52	2	5.06±0.0	5.7	269.54±29.97	16.06	Non-Dispersible
Pe-HA	96	2	5.17±1.4	3.8	354.41±0.94	30.53	Non-Dispersible
Kaltostat ^a	-	-	18.44±1.3	350	148±4.2	-	Dispersible

^a from reference (Uzun et al., 2013)

^b the smallest diameter of the cylinder which caused no crack on the film.

The testing method used to determine the flexibility of polymer coating materials was adapted to hydrogels in our study. For this purpose, the pectin hydrogel was first fixed to a rectangular tin plate and rolled on the plate test device to observe whether there were any cracks. The diameter of the smallest cylinder that did not cause cracking in the film was determined. Since both films did not crack after bending with the smallest diameter (2 mm) roller, they were determined to be quite flexible according to the applied test (Table 3). In summary, Pe and Pe-HA are quite flexible for a wound dressing application. These results are an indication that Pe-HA hydrogel films can be used easily during wound healing applications.

The absorbencies (liquid retention amount) of Pe and Pe-HA are given in Table 3, together with the absorbance of Kaltostat. Pe and Pe-HA retained liquid almost five times their dry mass. Their fluid retention capacity is approximately four times lower than that of Kaltostat. On the other hand, typical wound dressings show only 2.3% water absorption. Therefore, the liquid retention capacities of pectin and HA-based hydrogels are acceptable for wound dressing applications.

The rate of dehydration is an indicator of the formation of a moist wound environment along with its fluid retention capacity. As shown in Table 3, the dehydration rate of Pe

was found to be 58 times lower than that of the commercial product, and that of Pe-HA was 60 times lower. As mentioned in the previous paragraph, Kaltostat adsorbed four times more liquid than pectin-based hydrogels. This means that Kaltostat adsorbs much more liquid than Pe and Pe-HA films, but also loses much more water by evaporation. Considering the dehydration rate and liquid retention capacity of the samples together, it is predicted that our Pe-HA films will provide a more humid environment than Kaltostat, which is an advantage for wound healing.

While water loss from healthy skin is approximately 204±12 g.m⁻².day⁻¹, in injured skin, such as first-degree burns, this value varies between 279±26 and 5138±202 g.m⁻².day⁻¹ (Balakrishnan et al., 2005). An ideal wound dressing should keep water at an optimum level. It should keep the wound environment moist and prevent the removal of large amounts of water from the environment.

When Figure 8 is examined, it is seen that there is no significant change in water vapor permeability with the addition of HA to the matrix. The average water vapor permeability of 6 days for pectin was calculated as approximately 175 g.m⁻².day⁻¹, and for Pe-HA it was approximately 159 g.m⁻².day⁻¹. Notably, these values closely resemble the water vapor permeability of healthy skin. This finding underscores the potential of HA-Pe hydrogel films as

promising candidates for applications where maintaining an ideal moisture balance is crucial, such as wound healing and skin care.

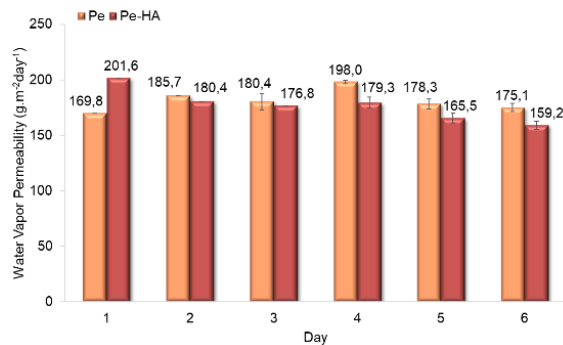


Figure 8. Average water vapor permeability of Pe and Pe-HA for 6 days.

As a result of adding HA to the Pe film, the average mass per unit area increased in Pe-HA films (Table 3). This change is notable in terms of thickness; while the average thickness for Pe is 0.13 mm, it increases to 0.16 mm for Pe-HA.

Film transparency is generally affected by additives in films, processing conditions, thickness, and compatibility between components. Transparency values of 16.06 for Pe and 30.53 for Pe-HA were reached (Table 3). According to these results, the transparency value increased as expected with the addition of HA. The increase in the weight per unit area for Pe-HA is also a reason for the increase in transparency in the film.

It was observed that Pe and Pe-HA did not disperse in the salt solution (Table 3). On the other hand, it is reported in the literature that the Kaltostat dressing completely disintegrates. One of the most studied topics is increasing the mechanical strength of wound dressings. For example, the mechanical properties of alginate-based dressing hydrogels increased with the addition of chitosan for infected chronic wounds and diabetic foot ulcers, as observed by Kurhade et.al (Kurhade et al., 2013) According to the results obtained, the synthesized hydrogel dressings (Pe and Pe-HA) had visual and mechanical properties under test conditions. Figure 9 provides visual information about the transparency of the films, and it was observed that the film's integrity was not damaged. This feature will provide a great advantage when removing the prepared hydrogels from the wound.

Conclusion

This study indicates the substantial potential for wound dressing applications of pectin-based hydrogel films supplemented with hyaluronic acid. The data suggest that these hydrogel films can be used effectively during wound therapy. The study's findings show that Pe-HA hydrogels have great flexibility, enough water absorption capacity, and a significant advantage in maintaining the moisture balance surrounding wounds. Furthermore, the water vapor

permeability of these films is comparable to that of healthy skin. These outcomes propose that Pe-HA hydrogel films hold promise for applications in wound treatment, skincare, and related fields. To conclude, hyaluronic acid-enriched pectin hydrogel films may offer a promising option in the field of wound treatment.

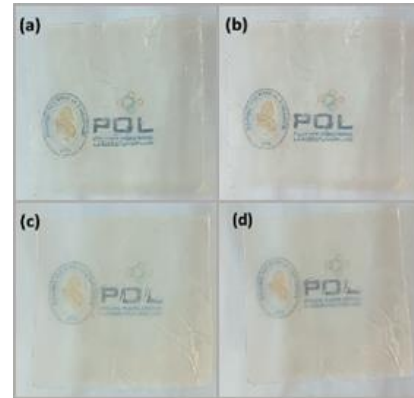


Figure 9. Photographs showing the dispersion properties of the prepared hydrogels: (a) Pe dry, (b) Pe wet, (c) Pe-HA dry, (d) Pe-HA wet.

Conflict of Interest

The authors declare that they have no conflicts of interest with respect to the research, authorship, and publication of this paper.

Funding Sources

This work was funded by The Scientific and Technological Research Council of Turkey (TUBITAK) with a project number of 20AG029.

References

- American Society for Testing and Materials. (2015). ASTM D2240-15 Standard Test Methods for Rubber Property-Durometer Hardness. *Annual Book of ASTM Standards*, 1–13. <https://doi.org/10.1520/D2240-15.2>
- Andriotis, E. G., Eleftheriadis, G. K., Karavasili, C., & Fatouros, D. G. (2020). Development of bio-active patches based on Pectin for the treatment of Ulcers and wounds using 3D-bioprinting technology. *Pharmaceutics*, 12(1). <https://doi.org/10.3390/pharmaceutics12010056>
- Balakrishnan, B., Mohanty, M., Umashankar, P. R., & Jayakrishnan, A. (2005). Evaluation of an in situ forming hydrogel wound dressing based on oxidized alginate and gelatin. *Biomaterials*, 26(32), 6335–6342. <https://doi.org/10.1016/j.biomaterials.2005.04.012>
- Bozer, B. M., Özkahraman, B., & Mert, H. (2023).

- Photocrosslinked methacrylated pectin and methacrylated hyaluronic acid wound dressing loaded with oleuropein as a bioactive agent. *International Journal of Polymeric Materials and Polymeric Biomaterials*, 0(0), 1–13. <https://doi.org/10.1080/00914037.2023.2235875>
- Chauhan, N., Saxena, K., & Jain, U. (2022). Hydrogel based materials: A progressive approach towards advancement in biomedical applications. *Materials Today Communications*, 33(September), 104369. <https://doi.org/10.1016/j.mtcomm.2022.104369>
- Conshohocken, W. (1996). ASTM E 96 - 00 Standard Test Methods for Water Vapor Transmission of Materials. *Current*, 91(Reapproved), 98–100.
- de Oliveira, S. A., da Silva, B. C., Riegel-Vidotti, I. C., Urbano, A., de Sousa Faria-Tischer, P. C., & Tischer, C. A. (2017). Production and characterization of bacterial cellulose membranes with hyaluronic acid from chicken comb. *International Journal of Biological Macromolecules*, 97, 642–653. <https://doi.org/10.1016/j.ijbiomac.2017.01.077>
- Divyashri, G., Badhe, R. V., Sadanandan, B., Vijayalakshmi, V., Kumari, M., Ashrit, P., Bijukumar, D., Mathew, M. T., Shetty, K., & Raghu, A. V. (2022). Applications of hydrogel-based delivery systems in wound care and treatment: An up-to-date review. *Polymers for Advanced Technologies*, 33(7), 2025–2043. <https://doi.org/10.1002/pat.5661>
- Farahnaky, A., Sharifi, S., Imani, B., Dorodmand, M. M., & Majzoobi, M. (2018). Physicochemical and mechanical properties of pectin-carbon nanotubes films produced by chemical bonding. *Food Packaging and Shelf Life*, 16(January), 8–14. <https://doi.org/10.1016/j.fpsl.2018.01.004>
- Galkowska, D., Długosz, M., Juszczak, L., Takamine, K., Abe, J., Shimono, K., Sameshima, Y., Morimura, S., Kida, K., & Sriamornsak, P. (2003). Chemistry of Pectin and Its Pharmaceutical Uses : A Review. *Silpakorn University Open Journal Systems*, 3(4), 206–228.
- Grkovic, M., Stojanovic, D. B., Kojovic, A., Strnad, S., Kreze, T., Aleksic, R., & Uskokovic, P. S. (2015). Keratin-polyethylene oxide bio-nanocomposites reinforced with ultrasonically functionalized graphene. *RSC Advances*, 5(111), 91280–91287. <https://doi.org/10.1039/c5ra12402f>
- Güner, O. Z., Cam, C., Arabacioglu-Kocaaga, B., Batirel, S., & Güner, F. S. (2018). Theophylline-loaded pectin-based hydrogels. I. Effect of medium pH and preparation conditions on drug release profile. *Journal of Applied Polymer Science*, 135(38), 1–12. <https://doi.org/10.1002/app.46731>
- Güner, O. Z., Kocaaga, B., Batirel, S., Kurkcuoglu, O., & Güner, F. S. (2021). 2-Thiobarbituric acid addition improves structural integrity and controlled drug delivery of biocompatible pectin hydrogels. *International Journal of Polymeric Materials and Polymeric Biomaterials*, 70(10), 703–711. <https://doi.org/10.1080/00914037.2020.1760272>
- Kafedjiiski, K., Jetti, R. K. R., Föger, F., Hoyer, H., Werle, M., Hoffer, M., & Bernkop-Schnürch, A. (2007). Synthesis and in vitro evaluation of thiolated hyaluronic acid for mucoadhesive drug delivery. *International Journal of Pharmaceutics*, 343(1–2), 48–58. <https://doi.org/10.1016/j.ijpharm.2007.04.019>
- Kumar, P. T. S., Ramya, C., Jayakumar, R., Nair, S. kumar V., & Lakshmanan, V. K. (2013). Drug delivery and tissue engineering applications of biocompatible pectin-chitin/nano CaCO₃ composite scaffolds. *Colloids and Surfaces B: Biointerfaces*, 106, 109–116. <https://doi.org/10.1016/j.colsurfb.2013.01.048>
- Kurhade, S., Momin, M., Khanekar, P., & Mhatre, S. (2013). Novel biocompatible honey hydrogel wound healing sponge for chronic ulcers. *International Journal of Drug Delivery*, 5(4), 353–361.
- Liao, Q., Kulkarni, Y., Sengupta, U., Petrović, D., Mulholland, A. J., Van Der Kamp, M. W., Strodel, B., & Kamerlin, S. C. L. (2018). Loop Motion in Triosephosphate Isomerase Is Not a Simple Open and Shut Case. *Journal of the American Chemical Society*, 140(46), 15889–15903. <https://doi.org/10.1021/jacs.8b09378>
- Martucci, J. F., & Ruseckaite, R. A. (2010). Biodegradable three-layer film derived from bovine gelatin. *Journal of Food Engineering*, 99(3), 377–383. <https://doi.org/10.1016/j.jfoodeng.2010.02.023>
- Mero, A., & Campisi, M. (2014). Hyaluronic acid bioconjugates for the delivery of bioactive molecules. *Polymers*, 6(1), 346–369. <https://doi.org/10.3390/polym6020346>
- Methods, S. T. (2001). ASTM D 522: Standard Test

- Methods for Mandrel Bend Test of Attached Organic Coatings. *ASTM International, Reapproved*, 1–4.
- Price, R. D., Myers, S., Leigh, I. M., & Navsaria, H. A. (2005). The Role of Hyaluronic Acid in Wound Healing. *American Journal of Clinical Dermatology*, 6(6), 393–402. <https://doi.org/10.2165/00128071-200506060-00006>
- Tarusha, L., Paoletti, S., Travan, A., & Marsich, E. (2018). Alginate membranes loaded with hyaluronic acid and silver nanoparticles to foster tissue healing and to control bacterial contamination of non-healing wounds. *Journal of Materials Science: Materials in Medicine*, 29(3). <https://doi.org/10.1007/s10856-018-6027-7>
- Taufiq, M., & Saifullah, B. I. N. (2019). *Optimization of Pectin Extraction From. January*, 1–13.
- Updated, L., En, T., This, F. A. C., Tm-, S., Capacity, F. H., Handling, F., & This, C. (2016). EN 13726 Primary Wound Dressing Test Methods. *British and European Standard Test Methods, January 2011*. <http://www.smtl.co.uk/testing-services/54-wound-dressings-testing-services/127-primary-wound-dressings.html>
- Uzun, M., Anand, S. C., & Shah, T. (2013). In Vitro Characterisation and Evaluation of Different Types of Wound Dressing Materials. *Journal of Biomedical Engineering and Technology*, 1(1), 1–
7. <https://doi.org/10.12691/jbet-1-1-1>
- Wang, S. Bin, Chen, A. Z., Weng, L. J., Chen, M. Y., & Xie, X. L. (2004). Effect of Drug-loading Methods on Drug Load, Encapsulation Efficiency and Release Properties of Alginate/Poly-L-Arginine/Chitosan Ternary Complex Microcapsules. *Macromolecular Bioscience*, 4(1), 27–30. <https://doi.org/10.1002/mabi.200300043>
- Wang, W., Ma, X., Jiang, P., Hu, L., Zhi, Z., Chen, J., Ding, T., Ye, X., & Liu, D. (2016). Characterization of pectin from grapefruit peel: A comparison of ultrasound-assisted and conventional heating extractions. *Food Hydrocolloids*, 61, 730–739. <https://doi.org/10.1016/j.foodhyd.2016.06.019>
- Yang, W., Xu, H., Lan, Y., Zhu, Q., Liu, Y., Huang, S., Shi, S., Hancharou, A., Tang, B., & Guo, R. (2019). Preparation and characterisation of a novel silk fibroin/hyaluronic acid/sodium alginate scaffold for skin repair. *International Journal of Biological Macromolecules*, 130, 58–67. <https://doi.org/10.1016/j.ijbiomac.2019.02.120>
- Zhou, Z., Chen, J., Peng, C., Huang, T., Zhou, H., Ou, B., Chen, J., Liu, Q., He, S., Cao, D., Huang, H., & Xiang, L. (2014). Fabrication and physical properties of gelatin/sodium alginate/hyaluronic acid composite wound dressing hydrogel. *Journal of Macromolecular Science, Part A: Pure and Applied Chemistry*, 51(4), 318–325. <https://doi.org/10.1080/10601325.2014.882693>

Visible Light-Induced Fabrication of a Clickable Cu(I) Benzophenone Dicarboxylate Polymer - Polyacrylamide Hydrogel Composite

Sena Ermiş¹, Mehmet Bilgiç Bilgehan² , Barış Kışkan^{1*}  and Kerem Kaya^{1*} 

¹ Istanbul Technical University, Chemistry Department, Maslak, 34469 İstanbul, Türkiye

² Wood Coating R&D Centre, Kubilay Boya, Aliağa, 35800 İzmir, Türkiye

Abstract: Hydrogels are a class of hydrophilic polymers that have been widely applied in numerous fields, most of which are related to bioengineering such as tissue scaffolds, biosensing, and antibacterial activity. Especially, polyacrylamide (PAAm) hydrogels, due to their superior stability, non-toxicity, and viscoelasticity, have been extensively studied over the last two decades in different bio-related applications. Coordination polymers (CPs) including metal-organic frameworks (MOFs), due to tunability of the organic linkers and metal ions, and their robustness, have been incorporated with hydrogels in order to improve the physical/chemical properties of the final composite. Herein, we report, for the first time, the utilization of a photoactive Cu(I) coordination polymer as a Norrish type II photoinitiator for the in situ fabrication of a clickable and highly-crosslinked Cu(I)CP-PAAm hydrogel composite under visible light-induced conditions, employing water as the solvent. Due to the high stability of the Cu(I)CP in water, that was demonstrated by powder X-ray studies, the release of copper ions was observed to occur after more than two days. Another advantage of the developed synthetic method is the facile post-modification of the hydrogel composite by utilizing an azide-functionalized polymer through an internal copper-catalyzed azide-alkyne click reaction.

Keywords: Hydrogels, polyacrylamide, coordination polymers, light-induced polymerization, Type II photoinitiator.

Görünür Işık Altında Klık Tepkimesine Girebilecek Cu(I) Benzofenon Dikarboksilat Polimeri-Poliakrilamid Hidrojel Kompozitinin Eldesi

Özet: Hidrojeller doku mühendisliğinden, biyosensörlere ve antibakteriyel araştırmalara kadar geniş bir biyomühendislik uygulama alanına sahip hidrofilik polimerlerdir. Özellikle poliakrilamid (PAAm) hidrojeller, sahip oldukları düşük toksisite, yüksek stabilite ve viskoelastisite nedeniyle son 20 yılda birçok biyo-iliskili alanda yoğun bir şekilde denenmişlerdir. Öte yandan, koordinasyon polimerleri (CPs) ve onların alt sınıfı olan metal-organik çerçeveler (MOFs), sahip oldukları sağlamlık ve organik ligand/metal iyonlarının rahatça değiştirilebilmesinden dolayı hidrojellerle karıştırılmış ve ortaya üstün fiziksel ve kimyasal özelliklere sahip kompozit malzemeler çıkmıştır. Bu çalışmada, Cu(I) bir koordinasyon polimeri, ilk defa bir tip II fotobaşlatıcı olarak kullanılarak, görünür ışık *altında in situ* olarak yüksek çapraz bağlanma oranına sahip bir Cu(I)CP-PAAm hidrojel kompozitinin sentezi, çözücü su olmak üzere gerçekleştirilmiştir. Sentezlenen Cu(I)CP'nin sudaki yüksek stabilitesi X-ışını toz difraksiyonu yöntemiyle kanıtlanmış ve bu sayede bakır iyonlarının yavaş salınımı gözlemlenmiştir. Ortaya atılan bu yeni sentetik yöntemin bir başka avantajıysa Cu(I)CP'nin kendi içinde bulundurduğu bakırın katalizör olarak kullanılabilmesi sayesinde kompozitin herhangi azid uçlu başka bir polimer ile azid-alkin klık tepkimesi üzerinden post-modifiye edilebilme potansiyeline sahip olmasıdır.

Anahtar Kelimeler: Hidrojeller, poliakrilamid, koordinasyon polimerleri, ışık-başlatmalı polimerleşme, Tip II fotobaşlatıcı.

RESEARCH PAPER

Corresponding Authors: Barış Kışkan, kiskanb@itu.edu.tr, Kerem Kaya, kkaya@itu.edu.tr.

Citation: Ermiş, S., Bilgehan, M. B., Kışkan, B., Kaya, K., (2024), Visible Light-Induced Fabrication of a Clickable Cu(I) Benzophenone Dicarboxylate Polymer - Polyacrylamide Hydrogel Composite, ITU ARI Bulletin of the Istanbul Technical University 55(2) 23–28.

Submission Date : 17 December 2023
Online Acceptance : 3 February 2024
Online Publishing : 3 February 2024

1.Introduction

Hydrogels are chemically and/or physically cross-linked 3D hydrophilic macromolecules that are capable to absorb large quantities of water without dissolving (Ahmed, 2015; Cao et al., 2021). Their hydrophilicity is attributed to the functional groups they contain, such as -OH, -NH₂, -COOH, -SO₃, and -CONH₂. Besides their ability to hold large water content, hydrogels are considered as biocompatible and have no or very little organism invasion (Yu et al., 2018). All these features have recently rendered hydrogels, a distinct class of materials that found great use in many bio-related applications including drug carriers (Vigata et al., 2020),

biomolecular supports (Heo & Crooks, 2005), nano-reactors (Soto-Quintero et al., 2017) and tissue scaffolds (Zhang et al., 2018).

Gelatin, chitosan, agarose, and alginate are the mostly known naturally occurring hydrogels that have been well studied (Taghipour et al., 2020). Among synthetic hydrogels, particularly polyacrylamide (PAAm) hydrogels, due to their stability, swelling capacity, non-toxicity, non-immunogenicity and viscoelasticity, have been extensively investigated by many research groups (Orakdogan & Okay, 2006) (Ceylan et al., 2006) (Norioka et al., 2021). In the last two decades, PAAm hydrogels have found wide application as soft tissue fillers (Wang et al., 2022) and antibacterial

scaffolds (Dsouza et al., 2022). PAAm is a colorless hydrogel that can be combined with other molecules in order to tailor many of its properties like physical toughness, anti-bacterial activity, thus, finally obtain the desired features for the aimed application(s). One of the main drawbacks of PAAm hydrogels is their relatively low elastic modulus, thus low mechanical strength, limiting their standalone use in several applications which require robustness (Dsouza et al., 2022). In order to solve this problem, PAAm hydrogels have been combined with a variety of materials possessing better mechanical performances (Abdurrahmanoglu et al., 2011).

Coordination polymers (CPs) and their subclass of metal-organic frameworks (MOFs) are classes of materials formed by the connection of metal ions to organic linkers (binders). CPs have been immensely researched for potential applications like gas sensing, drug delivery, water purification, catalysis, and batteries (Engel & Scott, 2020). In addition, they have been also incorporated with hydrogels, including PAAm, to enhance the physical properties of the composite (Samav et al., 2023) (Al-Mahamad et al., 2017). Moreover, synthetic flexibility of the organic linkers and metal ions of CPs, brings a great versatility to the both physical and chemical features of the CP-hydrogel composite. Metal ions present inside CPs are generally in nano-size and non-biodegradable. While many transition metals are known to be highly toxic (lead, chromium, arsenic, cadmium), copper is one of the essential trace elements found in the human body and has been demonstrated to promote the proliferation of various cells and angiogenesis (Zhou et al., 2020). Furthermore, copper ions which are known to be bioactive, play critical roles in many anti-inflammatory actions due to their anti-bacterial properties (Tao et al., 2019). Latest studies have revealed excellent performance of copper-based MOF-hydrogel composites in skin wound healing (You et al., 2022). However, due to the considerable cytotoxicity of copper ions, achievement of their slow release is an important criterion for the bio-related applications of Cu-based CP-hydrogel composites (Xiao et al., 2017). Another drawback associated with CPs, is their instability in aqueous media, resulting in their gradual decomposition (Terzyk et al., 2019).

Regarding the synthetic methods for the transition metal CP-hydrogel composites, CPs are most of the time introduced into hydrogels either by *in situ* growth or by direct mixing methods (Lim et al., 2023). While *in situ* growth technique implies the growth of CP in the pores of a pre-prepared hydrogel network, the direct mixing method forms CP-hydrogel composites via physical encapsulation of CPs during the cross-linking or gelation process of the hydrogel matrix (Hou et al., 2023). Lately, new strategies have also been developed for the successful synthesis of CP-hydrogel composites (Sun et al., 2023).

One of the most promising strategies to obtain CP-hydrogel composite is to use light as the energy source. Especially after the environmental concerns related to pollution caused by high demand of energy, light-induced polymerization reactions have become sustainable tools to obtain industrially important materials (Sanchez-Rexach et al., 2020) (Kaya, 2023) (Tabak et al.) (Kocaarslan et al., 2022). Among the advantages brought to hydrogels by photochemical reactions stand rapid curing/gelation and excellent spatiotemporal control occurring at room temperature (Nguyen & West, 2002). Particularly, the use of visible light is crucial to acquire efficient curing due to higher penetration ability of visible light compared to UV light (Kalayci et al., 2020). Several hydrogels have been recently synthesized by our group under UV or visible light, by employing both Norrish type I and type II photoinitiators (Bilgic et al., 2022) (Murtezi et al., 2014) (Yilmaz et al., 2011) (Uygun et al., 2009).

In this work, for the first time, a benzophenone containing, visible

light active Cu(I) coordination polymer has been used as type II photoinitiator for the *in situ* synthesis/fabrication of a post-modifiable/clickable CP-PAAm hydrogel composite. The advanced approach possesses several advantages over the conventional methods such as the straightforwardness, avoiding the use of additional photoinitiator, high cross-linking, possibility of post-modification through internal (self-containing) copper-catalyzed azide-alkyne click chemistry, relatively stable nature of the Cu(I) CP and slow release of copper ions that was observed by the slow change in the color of the hydrogel-composite over time.

2. Materials and Methods

2.1 Materials

Propargyl acrylate (PA) (98%, Sigma) and triethylene glycol dimethacrylate (TEGDMA) (Sigma) were passed through a short column filled with neutral activated aluminium oxide (0.063–0.200 mm) prior to use in order to remove the inhibitors. Acrylamide (AAM, Sigma-Aldrich) and trimethylamine (TEA) (99%, Sigma), copper sulfate pentahydrate ($\text{CuSO}_4 \cdot 5\text{H}_2\text{O}$) (Merck, 98%), benzophenone-4,4'-dicarboxylic acid (Sigma, 95%) and glacial acetic acid (Merck, 100%), were all used as purchased. Distilled water was obtained by a reverse-osmosis system equipped with a VONTRON ULP2012-100 membrane.

2.2. Methods

2.2.1 Instrumentations

IR Measurements. Fourier-transform infrared (FTIR) spectra were recorded on Perkin–Elmer Spectrum One spectrometer with an ATR Accessory (ZnSe, PikeMiracle Accessory) and mercury cadmium telluride (MCT) detector. 16 scans were averaged.

PXRD Measurements. Crystallographic identifications were accomplished by powder X-ray diffraction (PXRD) method on a benchtop Rigaku Miniflex diffractometer with a Cu-K α radiation source operated at 30 kV and 10 mA. The acquisition angle ranged from 5° to 90° with 10°·min⁻¹ scan speed.

UV–vis Measurements. UV-vis diffuse reflectance spectroscopy was measured with a UV 2600 spectrophotometer from Shimadzu with the respective accessory (ISR-2600 integrating sphere) in the range of 250 to 800 nm against BaSO₄ as the background. The Shimadzu LabSolutions UV–Vis Software package was used for measurement control and data analysis.

DSC measurements were performed on a Perkin Elmer Diamond DSC 4000 with a heating rate of 10 K·min⁻¹ under nitrogen flow of 20 mL·min⁻¹.

TGA measurements were carried out with a PerkinElmer Diamond TA/TGA instrument at a heating rate of 10 °C/min from 25 to 900 °C under a nitrogen atmosphere with a flow rate of 40 mL·min⁻¹.

2.2.2 Synthesis of Cu(I)CP

Cu(I)CP was synthesized according to a previously reported method where excess of $\text{Cu}(\text{SO}_4) \cdot 5\text{H}_2\text{O}$ was mixed with benzophenone-4,4'-dicarboxylic acid in formic acid - *N,N*-dimethylformamide (DMF) mixture prior to heating inside a conventional oven at 85° C for 24 h (Bilgic et al., 2022).

2.2.3 Fabrication of Cu(I)CP-PAAm Hydrogel Composite

For the synthesis of the Cu(I)CP-PAAm hydrogel composite, 10

mg of Cu(I)CP, 142 mg of AAm (2.0 mmol), 10 μ L of PA (0.1 mmol), 25 μ L of TEGDMA (0.1 mmol) and drops of TEA were dissolved in 1 mL of distilled water inside a test tube. In order to obtain a homogeneous mixture, the tube was ultrasonicated for 10 minutes and then transferred into a 1000 μ L syringe. The syringe was irradiated horizontally, inside a photoreactor equipped with 6 lamps (Philips TL-D 18W Blue) emitting a nominal light at 450 nm with an intensity of 30 mW/cm² on the reaction medium. After the irradiation, the hydrogel composite formed inside the syringe was gently pushed by using low pressure to the plunger.

3. Results and Discussion

Our previous studies have demonstrated that, classical Norrish type I photoinitiators like Irgacure-2959, bis(acyl)phosphane oxide (BAPO), 2,2-dimethoxy-2-phenylacetophenone (DMPA), as well as type II initiators like camphorquinone could initiate the light-induced polymerization of AAm-PA mixture (Bilgic et al., 2022; Murtezi et al., 2014). For the case of type II photoinitiators, a co-catalyst possessing hydrogen donor ability such as tertiary amines or compounds containing ethyleneoxide moieties are necessary. Benzophenone and its derivatives are also well-established type II photoinitiators and all these initiators possess lower excited triplet state energy compared to their cleaved state, thus, they do not decompose but form radicals in the carbonyl moiety upon excitation in the wavelength they absorb (Liu et al., 2021).

In the present work, we used AAm and PA as monofunctional monomer and bifunctional monomer possessing both double and triple bonds, respectively, in conjunction with very small amounts of TEGDMA and TEA as cross-linking agent and co-catalyst, respectively. The different reaction rates of the photochemically generated radicals with double and triple bonds were demonstrated by laser flash photolysis studies (Ciftci et al., 2012). Inspired from our previous photopolymerization studies concerning hydrogel formation, we envisioned the use of Cu(I)CP as a type II photoinitiator, due to its benzophenone moiety, for the polymerization of AAm-PA mixture in conjunction with TEA as the co-catalyst. Figure 1 depicts the summary of the synthesis of Cu(I)CP together with the photopolymerization reaction leading to hydrogel composite.

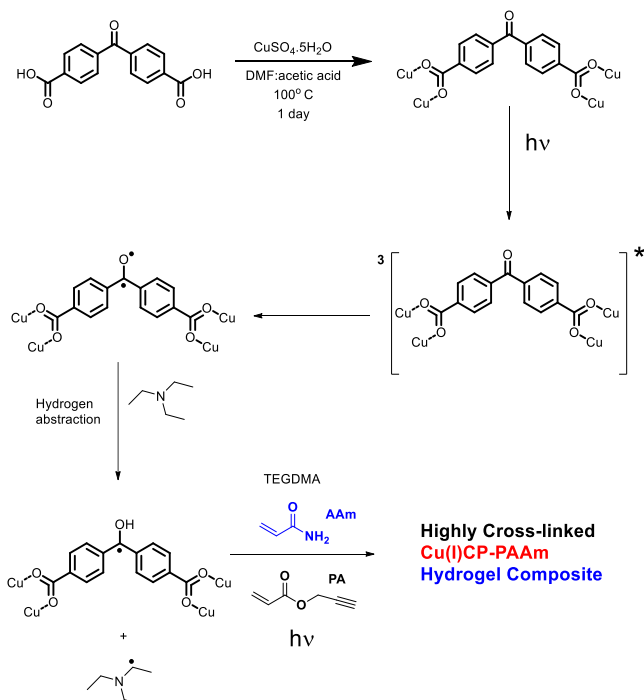


Figure 1. Light-induced fabrication of Cu(I)CP-PAAm hydrogel composite.

Although benzophenone itself absorbs light in the UV-A region, UV-Vis diffuse reflectance measurements of Cu(I)-CP powder exhibited a strong absorbance in the visible region (Figure 2). As mentioned in the introduction part, due to its higher penetrating ability (compared to UV), visible light is crucial for the rapid gelation during the photopolymerization reactions.

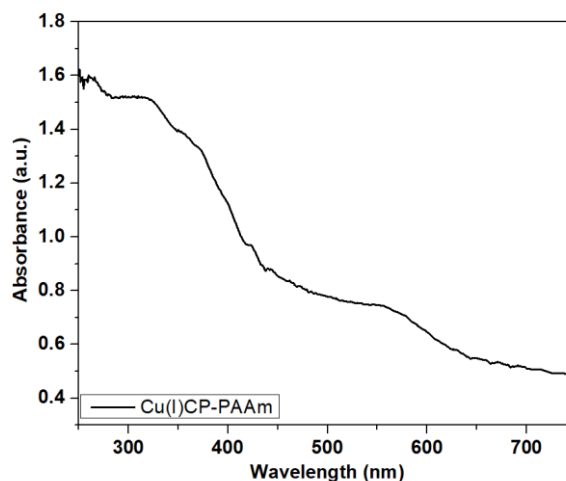


Figure 2. Diffuse reflectance UV-Vis spectrum of Cu(I)CP.

For the purification of the obtained hydrogel-composite, the composite was immersed in distilled water for five days, and then dried at room temperature. Photographs of the hydrogel composite (a) before and (b) after immersion to water for five days, are depicted in Figure 3.

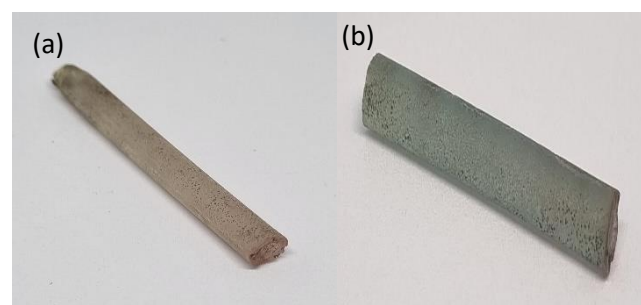


Figure 3. Photograph of the hydrogel composite (a) before (b) after immersion into water for five days.

Swelling degree of the hydrogel composite was calculated as 6.15% according to Equation 1.

$$\text{Eq. 1} = \text{Swelling (\%)} = (W_s (1.414 \text{ g}) - W_d (1.332 \text{ g})) / W_d (1.332 \text{ g}) \times 100 = 6.15$$

Where W_d = Weight of polymer and W_s = weight of swollen polymer.

Low degree of swelling of the photochemically synthesized hydrogel composite indicates a high cross-linking degree (Zhan et al., 2021), which was also encountered in the following results. The relatively stable nature of Cu(I)CP was demonstrated by powder X-ray analysis (PXRD) (Figure 4). In addition, it is possible to observe a clear coloring to blue in the hydrogel composite, after five days of immersion in water. This is attributed to the slow release of the Cu(II) ions in the form of Cu(OH)₂ giving a greenish blue color (Zhu et al., 2021). Cu(I) ions can easily be oxidized to Cu(II) ions in aqueous medium.

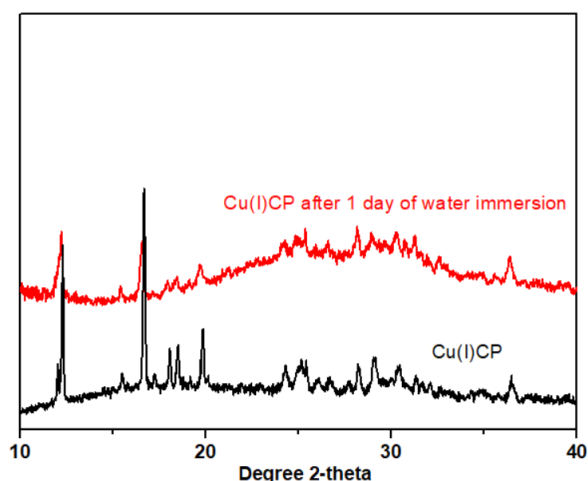


Figure 4. PXRD diffractograms of (black line) Cu(I)CP and (red line) Cu(I)CP after 1 day of immersion in water.

Following the swelling experiment, infrared (FTIR) investigation was employed in order to determine the functional groups present in the hydrogel composite (Figure 5). The composite IR spectrum displayed two different peaks in the carbonyl region; one at around 1650 cm^{-1} corresponding to the carbonyl of the benzophenone moiety of Cu(I)CP and a peak at ca. 1720 cm^{-1} corresponding to the carbonyls of PAAm, poly (propargylacrylate) and PEGDMA units. There is also a peak, although very weak, at around 2150 cm^{-1} belonging to the triple bond of the alkyne unit of PA. The weakness of the peak is attributed to several factors including the reaction between the triple bonds and the radicals formed by excitation, the relatively lower amount of PA used in the photoreaction mixture and low sensitivity of ZnSe crystal of ATR equipment on that region ($2000\text{--}2300\text{ cm}^{-1}$) (Aakeröy et al., 2013). Lastly in the IR spectrum, there is a very broad peak centered at 3400 cm^{-1} corresponding to the water absorbed by the hydrogel composite.

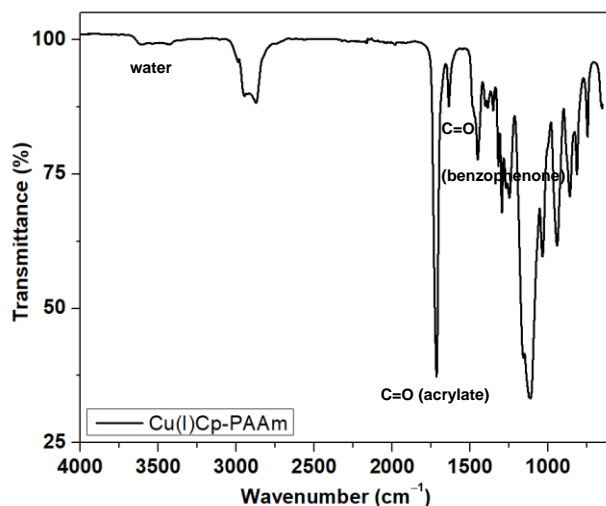


Figure 5. FTIR spectrum of the photochemically obtained hydrogel composite.

Differential scanning calorimetry (DSC) was performed on Cu(I)CP-PAAm hydrogel in order to investigate the thermal transitions (Figure 6). A large endotherm starting from around $70\text{ }^{\circ}\text{C}$ going until $110\text{ }^{\circ}\text{C}$ is due to the evaporation of large amount of water absorbed inside the hydrogel composite. In the DSC thermogram, besides this large endotherm, a weak endotherm at $202\text{ }^{\circ}\text{C}$ can be observed. This peak is attributed to the glass transition temperature (T_g) of PAAm and is due to the amorphous structure of PAAm. T_g of the previously synthesized PAAm hydrogels were observed around $190\text{ }^{\circ}\text{C}$ (Qin et al., 2016). The increase of the glass transition

temperature indicates a higher cross-linking degree and is also possibly related to the chemical incorporation of the Cu(I)CP into the PAAm hydrogel. After $275\text{ }^{\circ}\text{C}$, a large endotherm which corresponds to the initiation of the thermal degradation of the hydrogel composite, can be observed. This observation is in accordance with the thermal gravimetric analysis (TGA) and differential thermal analysis (DTA) data which will be discussed below (Figure 7).

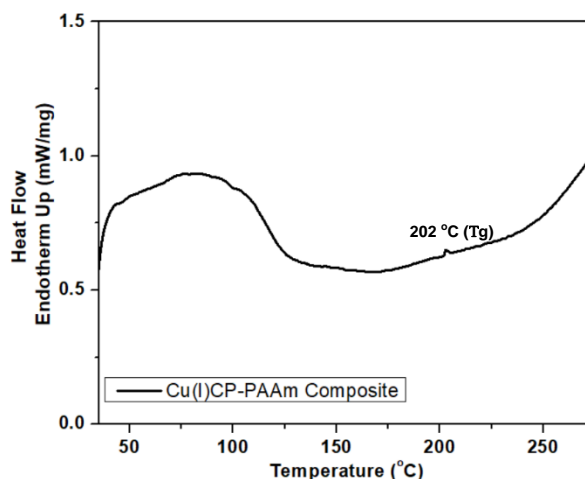


Figure 6. DSC thermogram of Cu(I)CP-PAAm hydrogel composite.

The thermal decomposition of Cu(I)CP, Cu(I)CP-PAAm hydrogel composite and PAAm hydrogel (synthesized using benzophenone instead of the coordination polymer), was carried out from $25\text{ }^{\circ}\text{C}$ to $800\text{ }^{\circ}\text{C}$ under nitrogen atmosphere with a heating rate of $20\text{ }^{\circ}\text{C min}^{-1}$. The corresponding TG curves can all be observed in Figure 7. The weight loss of the hydrogel composite can be roughly divided into three stages. Up until $110\text{ }^{\circ}\text{C}$, 5% weight loss can be observed. This is due to the evaporation of water absorbed by the hydrogel composite. After $110\text{ }^{\circ}\text{C}$, up until $250\text{ }^{\circ}\text{C}$, a second weight loss (5%) can be observed. This might be due to the evaporation of other reactants trapped inside the hydrogel network. After $250\text{ }^{\circ}\text{C}$, 60% weight loss (90% to 30%) occurs and this phenomenon is due to the gradual degradation of the hydrogel composite, which was also encountered in the DSC thermogram. From $450\text{ }^{\circ}\text{C}$ until $900\text{ }^{\circ}\text{C}$, there is only 0.5% weight left. This should belong to the copper present inside the hydrogel composite. Due to the lower crosslinking degree in PAAm synthesized by benzophenone, under UVA irradiation, especially until $300\text{ }^{\circ}\text{C}$, thermal stability of the composite is higher than pristine PAAm. This is attributed to the higher penetration ability of visible light over UVA light. Overall, thermal stability of the photochemically obtained PAAm hydrogel composite is much higher than pristine PAAm reported in the literature (Aydoğanlı et al., 2014) (Gün Gök & Inal, 2022).

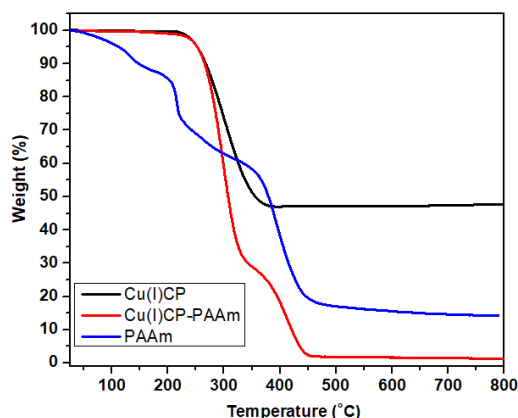


Figure 7. TGA thermograms of (blue) PAAm, (red) hydrogel composite, and (black) Cu(I)CP.

4. Conclusion

We have developed a straightforward and sustainable strategy for the light-induced *in situ* fabrication of a highly cross-linked copper(I) coordination polymer-polyacrylamide based hydrogel composite. The *in situ* generated hydrogel composite was thoroughly investigated by multiple spectroscopic and thermal analyses. DSC and TGA data displayed the improved thermal performance of the hydrogel composite, compared to pristine PAAm hydrogels. The novelty of the work is mainly the employment of a photoactive coordination polymer as a type II photoinitiator. Another advantage of the advanced approach is the possibility to post-modify the *in situ* generated hydrogel composite through the use of copper catalyzed azide-alkyne click chemistry. The presence of copper ions would avoid the necessity of additional copper species for the catalysis. We believe that the results of this work could open a new path for the sustainable fabrication of clickable hydrogels and can guide future research on copper containing hydrogels. The click reactions between the hydrogel composite and several azide species, are undergoing in our lab.

Acknowledgements








This work is dedicated to the memory of Professor Yusuf Yağcı. The authors acknowledge support from Istanbul Technical University Research Fund and YAP project-44004.

References

- Aakeröy, C. B., Baldrighi, M., Desper, J., Metrangolo, P., & Resnati, G. (2013). Supramolecular Hierarchy among Halogen-Bond Donors. *Chemistry – A European Journal*, 19(48), 16240-16247. <https://doi.org/https://doi.org/10.1002/chem.201302162>
- Abdurrahmanoglu, S., Cilingir, M., & Okay, O. (2011). Dodecyl methacrylate as a crosslinker in the preparation of tough polyacrylamide hydrogels. *Polymer*, 52(3), 694-699. <https://doi.org/https://doi.org/10.1016/j.polymer.2010.12.044>
- Ahmed, E. M. (2015). Hydrogel: Preparation, characterization, and applications: A review. *Journal of Advanced Research*, 6(2), 105-121. <https://doi.org/https://doi.org/10.1016/j.jare.2013.07.006>
- Al-Mahamad, L. L. G., El-Zubir, O., Smith, D. G., Horrocks, B. R., & Houlton, A. (2017). A coordination polymer for the site-specific integration of semiconducting sequences into DNA-based materials. *Nature Communications*, 8(1), 720. <https://doi.org/10.1038/s41467-017-00852-6>
- Aydinoğlu, D., Şen, S., Helvacıoğlu, E., Nugay, T., & Nugay, N. (2014). Tuning of heavy metal removal efficiency from water via micro algae/hydrogel composites. *e-Polymers*, 13. <https://doi.org/10.1515/epoly-2013-0116>
- Bilgic, M. B., Kaya, K., Orakdogan, N., & Yagci, Y. (2022). Light-induced synthesis and characterization of "Clickable" polyacrylamide hydrogels. *European Polymer Journal*, 167, 111062. <https://doi.org/https://doi.org/10.1016/j.eurpolymj.2022.111062>
- Cao, H., Duan, L., Zhang, Y., Cao, J., & Zhang, K. (2021). Current hydrogel advances in physicochemical and biological response-driven biomedical application diversity. *Signal Transduction and Targeted Therapy*, 6(1), 426. <https://doi.org/10.1038/s41392-021-00830-x>
- Ceylan, D., Ozmen, M. M., & Okay, O. (2006). Swelling–deswelling kinetics of ionic poly(acrylamide) hydrogels and cryogels. *Journal of Applied Polymer Science*, 99(1), 319-325. <https://doi.org/https://doi.org/10.1002/app.22023>
- Ciftci, M., Kahveci, M. U., Yagci, Y., Allonas, X., Ley, C., & Tar, H. (2012). A simple route to synthesis of branched and cross-linked polymers with clickable moieties by photopolymerization [10.1039/C2CC35607D]. *Chemical Communications*, 48(82), 10252-10254. <https://doi.org/10.1039/C2CC35607D>
- Dsouza, A., Constantinidou, C., Arvanitis, T. N., Haddleton, D. M., Charmet, J., & Hand, R. A. (2022). Multifunctional Composite Hydrogels for Bacterial Capture, Growth/Elimination, and Sensing Applications. *ACS Appl Mater Interfaces*, 14(42), 47323-47344. <https://doi.org/10.1021/acsami.2c08582>
- Engel, E. R., & Scott, J. L. (2020). Advances in the green chemistry of coordination polymer materials [10.1039/D0GC01074J]. *Green Chemistry*, 22(12), 3693-3715. <https://doi.org/10.1039/D0GC01074J>
- Gün Gök, Z., & Inal, M. (2022). Effective Removing of Remazol Black B by the Polyacrylamide Cryogels Modified with Polyethyleneimine. *Journal of Polymers and the Environment*, 30. <https://doi.org/10.1007/s10924-021-02187-2>
- Heo, J., & Crooks, R. M. (2005). Microfluidic biosensor based on an array of hydrogel-entrapped enzymes. *Anal Chem*, 77(21), 6843-6851. <https://doi.org/10.1021/ac0507993>
- Hou, X., Sun, J., Lian, M., Peng, Y., Jiang, D., Xu, M., Li, B., & Xu, Q. (2023). Emerging Synthetic Methods and Applications of MOF-Based Gels in Supercapacitors, Water Treatment, Catalysis, Adsorption, and Energy Storage. *Macromolecular Materials and Engineering*, 308(2), 2200469. <https://doi.org/https://doi.org/10.1002/mame.202200469>
- Kalayci, K., Frisch, H., Truong, V. X., & Barner-Kowollik, C. (2020). Green light triggered [2+2] cycloaddition of halochromic styrylquinoxaline—controlling photoreactivity by pH. *Nature Communications*, 11(1), 4193. <https://doi.org/10.1038/s41467-020-18057-9>
- Kaya, K. (2023). A green and fast method for PEDOT: Photoinduced step-growth polymerization of EDOT. *Reactive and Functional Polymers*, 182, 105464. <https://doi.org/https://doi.org/10.1016/j.reactfunctpolym.2022.105464>
- Kocaarslan, A., Kaya, K., Jockusch, S., & Yagci, Y. (2022). Phenacyl Bromide as a Single-Component Photoinitiator: Photoinduced Step-Growth Polymerization of N-Methylpyrrole and N-Methylindole. *Angewandte Chemie International Edition*, 61(36), e202208845. <https://doi.org/https://doi.org/10.1002/anie.202208845>
- Lim, J. Y. C., Goh, L., Otake, K.-i., Goh, S. S., Loh, X. J., & Kitagawa, S. (2023). Biomedically-relevant metal organic framework-hydrogel composites [10.1039/D2BM01906J]. *Biomaterials Science*, 11(8), 2661-2677. <https://doi.org/10.1039/D2BM01906J>
- Liu, S., Brunel, D., Noirbent, G., Mau, A., Chen, H., Morlet-Savary, F., Graff, B., Gimes, D., Xiao, P., Dumur, F., & Lalevée, J. (2021). New multifunctional benzophenone-based photoinitiators with high migration stability and their applications in 3D printing [10.1039/D0QM00885K]. *Materials Chemistry Frontiers*, 5(4), 1982-1994. <https://doi.org/10.1039/D0QM00885K>
- Murtezi, E., Ciftci, M., & Yagci, Y. (2014). Synthesis of

- Clickable Hydrogels and Linear Polymers by Type II Photoinitiation. *Polymer International*, 64. <https://doi.org/10.1002/pi.4786>
- Nguyen, K. T., & West, J. L. (2002). Photopolymerizable hydrogels for tissue engineering applications. *Biomaterials*, 23(22), 4307-4314. [https://doi.org/https://doi.org/10.1016/S0142-9612\(02\)00175-8](https://doi.org/https://doi.org/10.1016/S0142-9612(02)00175-8)
- Norioka, C., Inamoto, Y., Hajime, C., Kawamura, A., & Miyata, T. (2021). A universal method to easily design tough and stretchable hydrogels. *NPG Asia Materials*, 13(1), 34. <https://doi.org/10.1038/s41427-021-00302-2>
- Orakdogan, N., & Okay, O. (2006). Reentrant conformation transition in poly(N,N-dimethylacrylamide) hydrogels in water-organic solvent mixtures. *Polymer*, 47(2), 561-568. <https://doi.org/https://doi.org/10.1016/j.polymer.2005.11.066>
- Qin, H., Li, F., Wang, D., Lin, H., & Jin, J. (2016). Organized Molecular Interface-Induced Noncrystallizable Polymer Ultrathin Nanosheets with Ordered Chain Alignment. *ACS Nano*, 10(1), 948-956. <https://doi.org/10.1021/acsnano.5b06149>
- Samav, Y., Demir, S., Solmaz, G., Tuncer, C., & Erer, H. (2023). Construction of Novel Co(II) Coordination Polymers-Hydrogel Composites for Dye Adsorption. *Journal of Inorganic and Organometallic Polymers and Materials*, 1-12. <https://doi.org/10.1007/s10904-023-02882-8>
- Sanchez-Rexach, E., Johnston, T. G., Jehanno, C., Sardon, H., & Nelson, A. (2020). Sustainable Materials and Chemical Processes for Additive Manufacturing. *Chemistry of Materials*, 32(17), 7105-7119. <https://doi.org/10.1021/acs.chemmater.0c02008>
- Soto-Quintero, A., Romo-Uribe, A., Bermúdez-Morales, V. H., Quijada-Garrido, I., & Guarrotxena, N. (2017). 3D-Hydrogel Based Polymeric Nanoreactors for Silver Nano-Antimicrobial Composites Generation. *Nanomaterials (Basel)*, 7(8). <https://doi.org/10.3390/nano7080209>
- Sun, W., Zhao, X., Webb, E., Xu, G., Zhang, W., & Wang, Y. (2023). Advances in metal-organic framework-based hydrogel materials: preparation, properties and applications [10.1039/D2TA08841J]. *Journal of Materials Chemistry A*, 11(5), 2092-2127. <https://doi.org/10.1039/D2TA08841J>
- Tabak, T., Kaya, K., Isci, R., Ozturk, T., Yagci, Y., & Kiskan, B. Combining Step-Growth and Chain-Growth Polymerizations in One Pot: Light-Induced Fabrication of Conductive Nanoporous PEDOT-PCL Scaffold. *Macromolecular rapid communications*, n/a(n/a), 2300455. <https://doi.org/https://doi.org/10.1002/marc.202300455>
- Taghipour, Y. D., Hokmabad, V. R., Del Bakhshayesh, A. R., Asadi, N., Salehi, R., & Nasrabadi, H. T. (2020). The Application of Hydrogels Based on Natural Polymers for Tissue Engineering. *Curr Med Chem*, 27(16), 2658-2680. <https://doi.org/10.2174/0929867326666190711103956>
- Tao, B., Lin, C., Deng, Y., Yuan, Z., Shen, X., Chen, M., He, Y., Peng, Z., Hu, Y., & Cai, K. (2019). Copper-nanoparticle-embedded hydrogel for killing bacteria and promoting wound healing with photothermal therapy. *J Mater Chem B*, 7(15), 2534-2548. <https://doi.org/10.1039/c8tb03272f>
- Terzyk, A. P., Bieniek, A., Bolibok, P., Wiśniewski, M., Ferrer, P., da Silva, I., & Kowalczyk, P. (2019). Stability of coordination polymers in water: state of the art and towards a methodology for nonporous materials. *Adsorption*, 25(1), 1-11. <https://doi.org/10.1007/s10450-018-9991-9>
- Uygun, M., Kahveci, M. U., Odaci, D., Timur, S., & Yagci, Y. (2009). Antibacterial Acrylamide Hydrogels Containing Silver Nanoparticles by Simultaneous Photoinduced Free Radical Polymerization and Electron Transfer Processes. *Macromolecular Chemistry and Physics*, 210(21), 1867-1875. <https://doi.org/https://doi.org/10.1002/macp.200900296>
- Vigata, M., Meinert, C., Hutmacher, D. W., & Bock, N. (2020). Hydrogels as Drug Delivery Systems: A Review of Current Characterization and Evaluation Techniques. *Pharmaceutics*, 12(12). <https://doi.org/10.3390/pharmaceutics12121188>
- Wang, Y., Borthwell, R. M., Hori, K., Clarkson, S., Blumstein, G., Park, H., Hart, C. M., Hamad, C. D., Francis, K. P., Bernthal, N. M., & Phillips, K. S. (2022). In vitro and in vivo methods to study bacterial colonization of hydrogel dermal fillers. *J Biomed Mater Res B Appl Biomater*, 110(8), 1932-1941. <https://doi.org/10.1002/jbm.b.35050>
- Xiao, J., Chen, S., Yi, J., Zhang, H., & Ameer, G. A. (2017). A Cooperative Copper Metal-Organic Framework-Hydrogel System Improves Wound Healing in Diabetes. *Adv Funct Mater*, 27(1). <https://doi.org/10.1002/adfm.201604872>
- Yilmaz, G., Kahveci, M., & Yagci, Y. (2011). A One Pot, One Step Method for the Preparation of Clickable Hydrogels by Photoinitiated Polymerization. *Macromolecular rapid communications*, 32, 1906-1909. <https://doi.org/10.1002/marc.201100470>
- You, S., Xiang, Y., Qi, X., Mao, R., Cai, E., Lan, Y., Lu, H., Shen, J., & Deng, H. (2022). Harnessing a biopolymer hydrogel reinforced by copper/tannic acid nanosheets for treating bacteria-infected diabetic wounds. *Materials Today Advances*, 15, 100271. <https://doi.org/https://doi.org/10.1016/j.mtadv.2022.100271>
- Yu, S., Duan, Y., Zuo, X., Chen, X., Mao, Z., & Gao, C. (2018). Mediating the invasion of smooth muscle cells into a cell-responsive hydrogel under the existence of immune cells. *Biomaterials*, 180, 193-205. <https://doi.org/https://doi.org/10.1016/j.biomaterials.2018.07.022>
- Zhan, Y., Fu, W., Xing, Y., Ma, X., & Chen, C. (2021). Advances in versatile anti-swelling polymer hydrogels. *Materials Science and Engineering: C*, 127, 112208. <https://doi.org/https://doi.org/10.1016/j.msec.2021.112208>
- Zhang, K., Shi, Z., Zhou, J., Xing, Q., Ma, S., Li, Q., Zhang, Y., Yao, M., Wang, X., Li, Q., Li, J., & Guan, F. (2018). Potential application of an injectable hydrogel scaffold loaded with mesenchymal stem cells for treating traumatic brain injury [10.1039/C7TB03213G]. *Journal of Materials Chemistry B*, 6(19), 2982-2992. <https://doi.org/10.1039/C7TB03213G>
- Zhou, W., Zi, L., Cen, Y., You, C., & Tian, M. (2020). Copper Sulfide Nanoparticles-Incorporated Hyaluronic Acid Injectable Hydrogel With Enhanced Angiogenesis to Promote Wound Healing. *Front Bioeng Biotechnol*, 8, 417. <https://doi.org/10.3389/fbioe.2020.00417>
- Zhu, X., Chen, Y., Xie, R., Zhong, H., Zhao, W., Liu, Y., & Yang, H. (2021). Rapid Gelling of Guar Gum Hydrogel Stabilized by Copper Hydroxide Nanoclusters for Efficient Removal of Heavy Metal and Supercapacitors. *Front Chem*, 9, 794755. <https://doi.org/10.3389/fchem.2021.794755>

Strecker 3-Component Reaction for Post-Polymerization Modification of Pendant Aldehyde Functional Polymers

Mine Aybike Ersin¹ , Emre Akar¹ , Dilhan Kandemir¹ , Serter Luleburgaz¹ , Volkan Kumbaracı¹ ,
Ufuk Saim Gunay¹ , Hakan Durmaz^{1*} 

¹Department of Chemistry, Istanbul Technical University, 34469, Istanbul, Türkiye.

Abstract: Aldehydes have always been useful building blocks in organic chemistry due to their high and diverse reactivity. They also offer easy access to various other functionalities and allow reactions to be performed under mild conditions. This distinguished versatility has allowed aldehyde-bearing polymers to be a good platform for post-polymerization modification reactions to prepare functional polymers. This study exploited the Strecker 3-component reaction to obtain polymers with α -aminonitrile groups at the side chain for the first time. For this purpose, firstly, an aldehyde-functional polymer was synthesized from 4-formylphenyl methacrylate through free radical polymerization and then modified with amine compounds in the presence of trimethylsilyl cyanide and a catalytic amount of *p*-toluenesulfonic acid at room temperature. The spectroscopic analyses confirmed the successful synthesis of corresponding α -aminonitriles.

Keywords: Post-polymerization modification, Strecker 3-component reaction, aldehyde-functional polymers

Aldehit Yan Fonksiyonlu Polimerlerin Post-Polimerleşme Modifikasyonu için Strecker 3-Bileşenli Reaksiyonu

Özet: Aldehitler yüksek ve çeşitli reaktiviteleri nedeniyle organik kimyada her zaman yararlı yapı taşları olmuştur. Ayrıca, çeşitli diğer fonksiyonel gruplara kolay erişim sağlarlar ve reaksiyonların ılımlı koşullar altında gerçekleştirilmesine olanak tanırırlar. Bu seçkin çok yönlülük, aldehit taşıyan polimerlerin fonksiyonel polimerlerin hazırlanması amacıyla polimerizasyon sonrası modifikasyon reaksiyonları için iyi bir platform olmasına olanak sağlamıştır. Bu çalışma, ilk kez yan zincirde α -aminonitril gruplarına sahip polimerler elde etmek için Strecker 3-bileşenli reaksiyonundan yararlanmıştır. Bu amaçla öncelikle 4-formilfenil metakrilattan serbest radikal polimerizasyonu yoluyla aldehit fonksiyonlu bir polimer sentezlenmiş ve daha sonra oda sıcaklığında trimetilsilil siyanür ve katalitik miktarda *p*-toluensülfonik asit varlığında amin bileşikleriyle modifiye edilmiştir. Spektroskopik analizler, ilgili α -aminonitrillerin başarılı sentezini doğrulamıştır.

Anahtar Kelimeler: Polimerizasyon sonrası modifikasyon, Strecker 3-bileşenli reaksiyon, aldehit fonksiyonlu polimerler

RESEARCH PAPER

Corresponding Author: Hakan Durmaz, durmazh@itu.edu.tr

Citation: Ersin, A. M., Akar, E., Kandemir, D., Luleburgaz, S., Kumbaracı, İ. V., Gunay, U. S., Durmaz, H. (2024), Strecker 3-Component Reaction for Post-Polymerization Modification of Pendant Aldehyde Functional Polymers, ITU ARI Bulletin of the Istanbul Technical University 2024, 55(2) 29–36.

Submission Date : 28 December 2023

Online Acceptance : 13.02.2024

Online Publishing : 13.02.2024

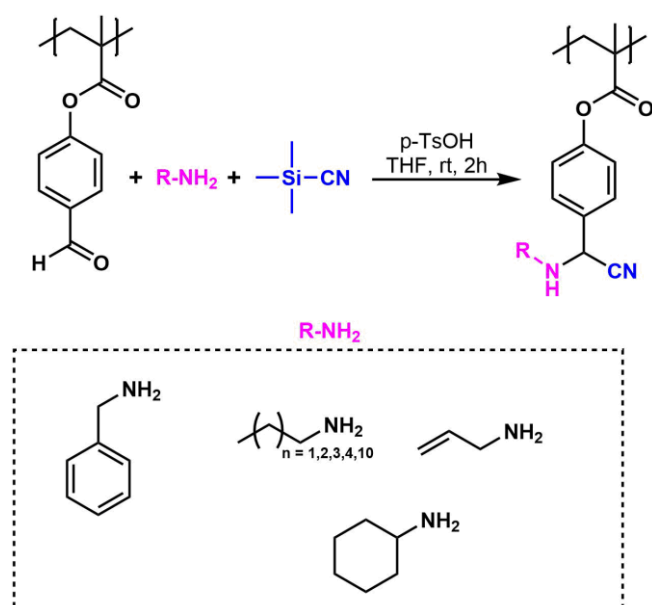
1.Introduction

Post-polymerization modification (PPM) is a crucial method in polymer chemistry, and it is significant for the synthesis of specifically designed functional polymers that could not be easily synthesized from corresponding functional monomers due to the possibility of losing the desired functionality under conventional polymerization conditions. "Click" reactions such as copper-catalyzed azide-alkyne cycloaddition (CuAAC) reaction, Diels-Alder reaction, thiol-yne/ene reactions, and multicomponent reactions (MCRs) are frequently used PPM tools (Geng et al., 2021; Blasco et al., 2017; Günay et al., 2013). Among them, MCRs are notably important in providing an atom-economic, fast, efficient, and less-waste-producing synthetic road, which makes them a good candidate for a "greener" chemistry approach (Zhi et al., 2019; Cioc Ersin, A. et al.

et al., 2014). Strecker 3-component reaction (S-3CR), introduced by Strecker (1850), is one of the oldest and most commonly studied MCRs where an aldehyde or a ketone, an amine, and a cyanide source are reacted to give α -aminonitriles which are an exceptionally important class of molecules not only because they are medicinally important but also because they can easily be converted to other biologically relevant molecules such as α -aminoacids, α -aminoalcohols, α -aminoketones/aldehydes, 1,2-diamines, and heterocyclic compounds (Kouznetsov & Galvis, 2018). In the classical S-3CR, aldehyde, amine, and highly toxic HCN or metal salts of cyanide are used in aqueous media. Over the years, many modifications have been made to S-3CR. Several less toxic cyanating agent alternatives such as trimethylsilyl cyanide

(TMSCN) (Liu et al., 2023; Shen et al., 2009), diethylphosphorocyanidate ((EtO)₂P(O)CN) (Harusawa & Shioiri, 2016), tributyltin cyanide (Bu₃SnCN) (Ishitani et al., 1998), diethylaluminum cyanide (Et₂AlCN) (Nakamura et al., 2004), and acetone cyanohydrin (ACH, CN(OH)CMe₂) (Sipos & Jablonkai, 2009) have been reported in the literature. TMSCN has several advantages, such as its good solubility in organic solvents, relatively safer nature, and better performance as a cyanating agent for imines under mild conditions (Xi et al., 2023). Also, it is known that many catalysts, from simple Bronsted acids such as *p*-toluenesulfonic acid (*p*-TsOH) (Reddy & Raghu, 2008) to Lewis acids like InCl₃ (Ranu et al., 2002) to complex macromolecular materials (Maleki et al., 2016), can catalyze S-3CR using TMSCN. Due to its inherent reactivity, the aldehyde group gives many valuable reactions easily under mild conditions ranging from imine/oxime/hydrazone formation to aldol reactions and MCRs and is frequently used in polymer chemistry for the synthesis of new types of polymers (Suesmatsu et al., 1983; Kreye et al., 2011; Kusumoto et al., 2013; Tunca, 2018; Negrell et al., 2018).

Pendant aldehyde functional polymers can be synthesized from the polymerization of aldehyde-functional monomers such as 4-vinylbenzaldehyde (Gao & Lam, 2008; Jackson et al., 2011) or 4-formylphenyl methacrylate (4FPM) (García-Acosta et al., 2007; Ravi Sankar et al., 2008; Kim et al., 2012) and can be used as PPM platforms. In a recent study (Akar et al., 2022), our group demonstrated that aldehyde-functional polymers can be easily modified via the reductive etherification reaction using alcohol or thiol nucleophiles in the presence of chlorodimethylsilane to obtain alkoxy- or thioether-/thioacetal-pendant polymers with high yields at room temperature. In this study, we aimed to further demonstrate the versatility of the aldehyde-functional polymers via S-3CR for the first time, using a range of amines, TMSCN, and *p*-TsOH catalyst to obtain polymers with α -aminonitrile moiety at the side chain. Scheme 1 depicts the general strategy followed in this study.



Scheme 1. General representation for the PPM of the aldehyde-functional polymer via S-3CR.

2. Experimental Part

2.1 Materials

4-Hydroxybenzaldehyde (98%, Sigma-Aldrich), methacryloyl chloride (97%, Sigma-Aldrich), triethylamine (≥ 99.5 , Sigma-Aldrich), azobis(cyclohexanecarbonitrile) (ABCN, 98%, Sigma-Aldrich), benzylamine (99%, Sigma-Aldrich), trimethylsilyl cyanide (TMSCN, 98%, Sigma-Aldrich), allylamine (98%, Sigma-Aldrich),

propylamine ($\geq 99\%$, Sigma-Aldrich), butylamine (99.5%, Sigma-Aldrich), pentylamine (99%, Fisher Scientific), hexylamine ($\geq 99.0\%$ Merck), dodecylamine ($\geq 99\%$, Sigma-Aldrich), cyclohexylamine ($\geq 99.5\%$, Sigma-Aldrich), *p*-toluenesulfonic acid monohydrate (*p*TsOH, 97%, Alfa Aesar), InCl₃ (98%, Sigma-Aldrich), trifluoroacetic acid (TFA, 99%, Sigma-Aldrich), hydrochloric acid (HCl, 37%, Sigma-Aldrich), sulfuric acid (H₂SO₄, 98%, Sigma-Aldrich), triflic acid (TfOH, $\geq 99\%$, Sigma-Aldrich) were used as received. Tetrahydrofuran (THF, $\geq 99.9\%$, Sigma-Aldrich), 1,4-dioxane ($\geq 99.5\%$, Sigma-Aldrich), chloroform (CHCl₃, $\geq 99\%$, Sigma-Aldrich), dimethyl sulfoxide (DMSO, $\geq 99.7\%$, Sigma-Aldrich), acetonitrile (CH₃CN, 99.8%, Sigma-Aldrich), and toluene (99.8%, Sigma-Aldrich) were anhydrous and were of HPLC quality, and used without further purification. Methanol, hexane and diethyl ether were of reagent grade and used without further purification.

2.2. Instrumentation

¹H NMR (500 MHz) and ¹³C NMR (125 MHz) spectra were recorded using an Agilent VNMR5 500 instrument in CDCl₃. Gel permeation chromatography (GPC) measurements were carried out with an Agilent Instrument (series 1100) using a refractive index detector loaded with Waters Styragel columns (HR 5E, HR 4E, HR 3, HR 2, 4.6 mm internal diameter, 300 mm length, packed with 5 μ m particles). The effective molecular weight ranges of the columns are 2000–4,000,000, 50–100,000, 500–30,000, and 500–20,000 g/mol, respectively. THF was used as an eluent at a flow rate of 0.3 mL/min at 30 °C, and 2,6-di-*tert*-butyl-4-methylphenol was used as an internal standard. The weight-average molecular weight (*M_w*) and dispersity (*Đ*) of the polymers were calculated based on narrow linear polystyrene (PS) standards (Polymer Laboratories) ranging between 2300 and 3,050,000 g/mol. FT-IR spectra were recorded on an Agilent Technologies Cary 630 FT-IR instrument over the range of 4000–400 cm⁻¹.

2.3. Synthetic Procedures

2.3.1. Synthesis of aldehyde-functional polymer (P0)

4-Formylphenyl methacrylate (4FPM) (6.58 g, 34.6 mmol) was added to a 50 mL Schlenk flask and dissolved in 33 mL of DMSO. Next, ABCN (0.42 g, 1.73 mmol) was added to this solution, and the reaction mixture was degassed by three freeze-pump-thaw cycles, left in a vacuum, and the mixture was allowed to stir at 80 °C for 14 h. After the specified time, the reaction mixture was cooled to room temperature, precipitated into 300 mL diethyl ether, and decanted. The dissolution-precipitation (CHCl₃-diethyl ether) process was repeated two times. The obtained polymer was finally dried in a vacuum oven for 24 h to give the P0 as a white powder (yield = 4.6 g, 70%). ¹H NMR (CDCl₃) δ 9.96 (s, 1H, CH=O), 7.81–7.24 (m, 4H, ArH), 2.26 – 1.42 (m, 5H, main backbone). ¹³C NMR (CDCl₃) δ 190.68, 174.64, 154.92, 134.29, 131.25, 121.73, 45.95, 20.33, 18.35.

2.3.2. General procedure for PPM of P0 via Strecker reaction

P0 (50 mg, 0.26 mmol based on repeating unit, 1 eq) was added to a 10 mL round-bottom flask and dissolved in 1 mL of THF. To this solution were added amine (0.52 mmol, 2 eq), TMSCN (0.39 mmol, 1.5 eq), and *p*-TsOH (0.026 mmol, 0.1 eq) in the given order. The mixture was then stirred at room temperature for 2 h. After that, the reaction mixture was directly precipitated into 20 mL of methanol or diethyl ether or diethyl ether:hexane (1:1, v:v) mixture, and the solvent was decanted. The dissolution-precipitation (CHCl₃-methanol or CHCl₃-diethyl ether or CHCl₃-diethyl ether:hexane (1:1, v:v)) process was repeated two times. Finally, the obtained polymer was dried in a vacuum oven at room temperature overnight.

2.3.3. Synthesis of P1

General procedure was followed. Benzylamine (57.4 μ L, 0.52 mmol), TMSCN (49.3 μ L, 0.39 mmol), and *p*-TsOH (5 mg, 0.026 mmol) were used. The mixture was precipitated into 20 mL of methanol to give P1 as a white solid (yield = 24 mg, 30%). ¹H NMR (CDCl₃) δ 8.30 (s, 1H, CH=N), 7.44 – 7.06 (m, 9H, ArH), 4.67 (m, 1H, CHCN), 3.97 – 3.86 (d, 2H, NCH₂Ph), 2.31 – 1.27 (m, 5H, main

backbone). ^{13}C NMR (CDCl_3) δ 174.58, 150.75, 137.98, 128.67, 127.69, 121.58, 118.53, 52.73, 51.20, 45.94.

2.3.4. Synthesis of P2

General procedure was followed. Propylamine (43.2 μL , 0.52 mmol), TMSCN (49.3 μL , 0.39 mmol), and *p*-TsOH (5 mg, 0.026 mmol) were used. The mixture was precipitated into 20 mL of methanol to give P2 as a white solid (yield = 38 mg, 57%). ^1H NMR (CDCl_3) δ 9.94 (s, 1H, $\text{CH}=\text{O}$), 8.25 (s, 1H, $\text{CH}=\text{N}$), 7.46 (s, 2H, ArH), 7.09 (s, 2H, ArH), 4.80 (m, 1H, CHCN), 3.57 (s, 2H, $\text{CH}=\text{NCH}_2$), 2.78-2.68 (m, 2H, $\text{CH}(\text{CN})\text{NHCH}_2$), 1.53-1.41 (m, 7H $\text{NCH}_2\text{CH}_2\text{CH}_3$ and main backbone), 0.95-0.84 (m, 3H, $\text{NCH}_2\text{CH}_2\text{CH}_3$). ^{13}C NMR (CDCl_3) δ 175.29, 159.59, 150.76, 132.90, 129.02, 125.81, 121.71, 118.87, 63.39, 53.90, 49.28, 45.74, 22.79, 11.66.

2.3.5. Synthesis of P3

General procedure was followed. Butylamine (52 μL , 0.52 mmol), TMSCN (49.3 μL , 0.39 mmol), and *p*-TsOH (5 mg, 0.026 mmol) were used. The mixture was precipitated into 20 mL of diethyl ether/hexane (1:1, v:v) to give P3 as a white solid (yield = 30 mg, 42%). ^1H NMR (CDCl_3) δ 8.25 (s, 1H, $\text{CH}=\text{N}$), 7.46 (m, 2H, ArH), 7.08 (m, 2H, ArH), 4.79 (m, 1H, CHCN), 2.82 - 2.71 (d, 2H, $\text{NCH}_2\text{CH}_2\text{CH}_2\text{CH}_3$), 2.36 (s, 2H, $\text{NCH}_2\text{CH}_2\text{CH}_2\text{CH}_3$), 1.56 - 1.39 (m, 8H, $\text{NCH}_2\text{CH}_2\text{CH}_2\text{CH}_3$ and main backbone), 0.92 (m, 3H, $\text{NCH}_2\text{CH}_2\text{CH}_2\text{CH}_3$). ^{13}C NMR (CDCl_3) δ 175.12, 159.46, 150.71, 129.00, 128.53, 125.85, 121.52, 118.90, 61.39, 53.92, 47.19, 39.73, 31.68, 29.86, 20.28, 13.92.

2.3.6. Synthesis of P4

The general procedure was followed. Pentylamine (61 μL , 0.52 mmol), TMSCN (49.3 μL , 0.39 mmol), and *p*-TsOH (5 mg, 0.026 mmol) were used. The mixture was precipitated into 20 mL of ether to give P4 as a white solid (yield = 20 mg, 27%). ^1H NMR (CDCl_3) δ 8.25 (s, 1H, $\text{CH}=\text{N}$), 7.46 (s, 2H, ArH), 7.08 (s, 2H, ArH), 4.79 (m, 1H, CHCN), 3.60 (m, 2H, $\text{CH}=\text{NCH}_2$), 2.83-2.71 (m, 2H, $\text{CH}(\text{CN})\text{NCH}_2$), 1.52-1.33 (m, 11H, $\text{NCH}_2(\text{CH}_2)_3\text{CH}_3$ and main backbone), 0.89 (m, 3H, $\text{NCH}_2(\text{CH}_2)_3\text{CH}_3$). ^{13}C NMR (CDCl_3) δ 150.62, 128.97, 128.59, 121.54, 118.96, 61.76, 53.92, 47.61, 29.29, 22.49, 14.03.

2.3.7. Synthesis of P5

The general procedure was followed. Hexylamine (69.5 μL , 0.52 mmol), TMSCN (49.3 μL , 0.39 mmol), and *p*-TsOH (5 mg, 0.026 mmol) were used. The mixture was precipitated into 20 mL of diethyl ether/hexane (1:1, v:v) to give P5 as a white solid (yield = 36 mg, 46%). ^1H NMR (CDCl_3) δ 8.25 (s, 1H, $\text{CH}=\text{N}$), 7.46 (s, 2H, ArH), 7.08 (s, 2H, ArH), 4.79 (m, 1H, CHCN), 3.59 (m, 2H, $\text{CH}=\text{NCH}_2$), 2.83 - 2.71 (d, 2H, $\text{CH}(\text{CN})\text{NHCH}_2$), 1.52 - 1.29 (m, 13H, $\text{NCH}_2(\text{CH}_2)_4\text{CH}_3$ and main backbone), 0.88 (m, 3H, $\text{NCH}_2(\text{CH}_2)_4\text{CH}_3$). ^{13}C NMR (CDCl_3) δ 175.25, 159.72, 150.81, 133.12, 128.38, 125.85, 121.55, 118.86, 61.78, 53.93, 47.68, 31.63, 29.59, 26.82, 22.58, 14.05.

2.3.8. Synthesis of P6

The general procedure was followed. Dodecylamine (121 μL , 0.52 mmol), TMSCN (49.3 μL , 0.39 mmol), and *p*-TsOH (5 mg, 0.026 mmol) were used. The mixture was precipitated into 20 mL of methanol to give P6 as a white solid (yield = 28 mg, 29%). ^1H NMR (CDCl_3) δ 9.98 (s, 1H, $\text{HC}=\text{O}$), 8.24 (s, 1H, $\text{CH}=\text{N}$), 7.45 (m, 2H, ArH), 7.07 (m, 2H, ArH), 4.78 (m, 1H, CHCN), 3.60 (s, 2H, $\text{CH}=\text{NCH}_2$), 2.84 - 2.71 (m, 2H, $\text{CH}(\text{CN})\text{NHCH}_2$), 1.69 - 1.26 (m, 25H, $\text{NCH}_2(\text{CH}_2)_{10}\text{CH}_3$ and main backbone), 0.88 (s, 3H, $\text{NCH}_2(\text{CH}_2)_{10}\text{CH}_3$). ^{13}C NMR (CDCl_3) δ 175.49, 159.79, 150.77, 133.04, 128.55, 121.69, 61.82, 53.96, 47.80, 31.92, 29.66, 27.22, 22.69, 14.14.

2.3.9. Synthesis of P7

The general procedure was followed. Allylamine (39.4 μL , 0.52 mmol), TMSCN (49.3 μL , 0.39 mmol), and *p*-TsOH (5 mg, 0.026 mmol) were used. The mixture was precipitated into 20 mL of diethyl ether to give P7 as a whitish-yellow solid (yield = 33 mg, 50%). ^1H

NMR (CDCl_3) δ 9.97 (s, 1H, $\text{HC}=\text{O}$), 8.28 (s, 1H, $\text{CH}=\text{N}$), 7.46 (s, 2H, ArH), 7.07 (s, 2H, ArH), 5.86 (s, 1H, $\text{NCH}_2\text{CH}=\text{CH}_2$), 5.33-5.19 (m, 2H, $\text{NCH}_2\text{CH}=\text{CH}_2$), 4.80 (m, 1H, CHCN), 4.25 (m, 2H, $\text{CH}=\text{NCH}_2\text{CH}=\text{CH}_2$), 3.39 (m, 2H, $\text{CH}(\text{CN})\text{NHCH}_2\text{CH}=\text{CH}_2$), 1.52 - 1.41 (m, 5H, main backbone). ^{13}C NMR (CDCl_3) δ 175.42, 160.68, 150.76, 140.81, 134.69, 129.02, 125.91, 120.92, 117.98, 52.81, 49.91, 46.04, 41.99, 30.92, 21.33.

2.3.10. Synthesis of P8

The general procedure was followed. Cyclohexylamine (60 μL , 0.52 mmol), TMSCN (49.3 μL , 0.39 mmol), and *p*-TsOH (5 mg, 0.026 mmol) were used. The mixture was precipitated into 20 mL of methanol to give P8 as a white solid (yield = 19 mg, 26%). ^1H NMR (CDCl_3) δ 9.98 (s, 1H, $\text{HC}=\text{O}$), 8.27 (s, 1H, $\text{CH}=\text{N}$), 7.65 (m, 2H, ArH), 7.06 (m, 2H, ArH), 4.83 (s, 1H, CHCN), 3.20 (s, 1H, $\text{CH}=\text{NCH}$), 2.84 (s, 1H, $\text{CH}(\text{CN})\text{NHCH}$), 1.98 - 1.26 (m, 15H, CH_2 of cyclohexyl ring and main backbone). ^{13}C NMR (126 MHz, CDCl_3) δ 175.18, 165.38, 152.02, 134.58, 129.31, 129.25, 121.16, 119.23, 69.90, 54.88, 51.01, 45.88, 34.36, 33.79, 31.92, 24.78.

3. Results and Discussion

The aldehyde-functionalized polymer was synthesized from 4-formylphenyl methacrylate (4FPM) monomer according to previously published study by our group (Akar et al., 2022). Briefly, 4-hydroxybenzaldehyde was reacted with methacryloyl chloride to obtain 4FPM, and the resulting monomer (i.e., 4FPM) was then polymerized via free radical polymerization (FRP) using the initiator 1,1-azobis(cyclohexanecarbonitrile) (ABCN) in DMSO at 80 °C for 14 h. The obtained polymer (P0) showed a high molecular weight ($M_w = 100$ kDa) with a broad polydispersity ($\text{PDI} = 2.33$), which can be expected due to the nature of the FRP. As shown in Fig. 2A, aldehyde proton ($\text{HC}=\text{O}$) and aromatic protons of P0 were detected at 9.96 and 7.81 - 7.24 ppm, respectively. Also, in the FT-IR spectrum of P0 given in Fig. 2C, the aldehyde $\text{C}=\text{O}$ stretching peak was observed at 1698 cm^{-1} , while the ester carbonyl peak was detected at 1750 cm^{-1} . These results confirmed that P0 was synthesized successfully. After the preparation of the aldehyde-functional polymer, a series of experiments were conducted to determine the optimum conditions for PPM of P0 via S-3CR. To this end, P0 was reacted with benzylamine (BA), trimethylsilyl cyanide (TMSCN), and *p*-toluenesulfonic acid (*p*-TsOH) in THF at room temperature for 2 h at different BA/TMSCN/*p*-TsOH mole ratios (Fig. 1 and Table 1).

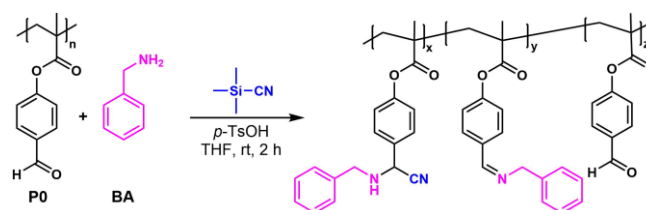


Fig. 1. Model reaction between P0 and BA and the resulting product distribution.

The conversion of aldehyde to the corresponding α -aminonitrile (α -AN) and imine products was calculated by comparing the integral ratios of benzylic methylene protons (NCH_2Ph) with the methine proton next to the cyano group (CHCN) and to the imine proton ($\text{CH}=\text{N}$) using ^1H NMR.

Table 1 Optimization studies of the reactants^a

Run	BA (eq) ^b	TMSCN (eq) ^b	<i>p</i> -TsOH (eq) ^b	<i>x/y/z</i> ^c
1	1.1	1.1	0.1	0.70/0.20/0.10
2	1.5	1.1	0.1	0.85/0.10/0.05
3	2	1.1	0.1	0.90/0.10/0
4	2	1.5	0.1	0.97/0.03/0
5	2	2	0.1	0.96/0.04/0
6	2	1.5	0.2	0.97/0.03/0
7	2	1.5	0.05	0.90/0.10/0

^aThe reactions were carried out in 1 mL of THF at room temperature for 2 h. ^bPer repeating unit of P0. ^cDetermined by ¹H NMR.

First, using equal moles of BA and TMSCN (1.1 eq each) per aldehyde unit of P0 in the presence of 0.1 eq of *p*-TsOH as catalyst resulted in the formation of α -AN with 70% conversion and imine with 20% conversion while leaving 10% unreacted aldehyde (Table 1, run 1). Increment of BA to 1.5 eq while keeping TMSCN and *p*-TsOH constant led to the formation of 85% α -AN and 10% imine, and 5% aldehyde remained unreacted (Table 1, run 2). Further increase of BA to 2 eq resulted in full consumption of the aldehyde; 90% of α -AN and 10% of imine were obtained at the end of the reaction (Table 1, run 3). Moreover, increasing TMSCN to 1.5 eq while keeping BA at 2 eq afforded near quantitative conversion (97%) of aldehyde to α -AN with only 3% imine product (Table 1, run 4). Similar α -AN conversion (96%) was obtained when increasing TMSCN to 2 eq (Table 1, run 5). These results indicate that the optimum equivalents of BA and TMSCN per aldehyde are 2/1.5 (BA/TMSCN). We also examined the effect of the acid catalyst equivalent on conversion. Increasing the acid equivalent to 0.2 eq using the optimum equivalents of the reactants given above led to the same α -AN conversion (97%) obtained in the 0.1 eq case (Table 1, run 6); however, lowering *p*-TsOH to 0.05 eq caused a slight decrease in the conversion (90%) (Table 1, run 7). Thus, the ideal mole ratio of BA/TMSCN/*p*-TsOH per aldehyde was found to be 2/1.5/0.1.

The effect of different acid catalysts on S-3CR was next examined using the optimum mole ratios of the reactants. It was found that *p*-TsOH still gave the best results (Table 2, run 1) with 97% α -AN formation, followed by trifluoroacetic acid (TFA), which led to the formation of α -AN with 62% conversion and imine product with 26% conversion, the remaining 12% was unreacted aldehyde (Table 2, run 2). Utilizing other acid catalysts, namely triflic acid (TfOH), InCl₃, HCl, and H₂SO₄, resulted in insoluble polymers that could not be characterized (Table 2, runs 3-6).

Table 2 Effect of different catalysts on Strecker reaction^a

Run	Catalyst	Efficiency (%) ^b
1	<i>p</i> -TsOH	97/3/0
2	TFA	62/26/12
3	TfOH	- ^c
4	InCl ₃	- ^c
5	HCl	- ^c
6	H ₂ SO ₄	- ^c

^aReactions were carried out using BA/TMSCN/catalyst at a mole ratio of 2/1.5/0.1 per repeating unit of P0 in 1 mL of THF at room temperature for 2 h. ^bMole ratios of α -aminonitrile/imine/aldehyde segments in the resulting polymer were determined by ¹H NMR. ^cInsoluble polymer was obtained.

Finally, the effect of different solvents on the reaction was examined. As can be seen in Table 3, THF was still the best

solvent with 97% α -AN formation (Table 3, run 1), followed by another cyclic ether-type solvent 1,4-dioxane which showed slightly lower efficiency with 95% α -AN and 5% imine product (Table 3, run 2). Using a relatively less polar halogenated solvent CHCl₃ resulted in only 40% α -AN formation along with 28% imine product and 32% unreacted aldehyde (Table 3, run 3). Other solvents, namely CH₃CN and toluene, gave insoluble polymers which could not be characterized (Table 3, runs 4-5).

Table 3 Effect of different solvents on Strecker reaction^a

Run	Solvent	Efficiency (%) ^b
1	THF	97/3/0
2	1,4-dioxane	95/5/0
3	CHCl ₃	40/28/32
4	CH ₃ CN	- ^c
5	Toluene	- ^c

^aReactions were carried out using BA/TMSCN/*p*-TsOH at a mole ratio of 2/1.5/0.1 per repeating unit of P0 in 1 mL of solvent at room temperature for 2 h. ^bMole ratios of α -aminonitrile/imine/aldehyde segments in the resulting polymer were determined by ¹H NMR. ^cInsoluble polymer was obtained.

Given all these results, it was found that the optimum mole ratio of reactants for PPM reactions *via* S-3CR was found to be 2/1.5/0.1 (BA/TMSCN/*p*-TsOH) per repeating unit of P0 in THF at room temperature for 2 h.

The ¹H NMR spectrum of the modified polymer (P1) (Table 1, run 4) is given in Fig. 2B. Complete disappearance of HC=O peak at 9.96 ppm confirms the quantitative conversion of aldehyde to corresponding α -AN and imine products. Benzylic methylene protons were detected at 3.86 - 3.97 ppm. Comparison of CHCN and CH=N protons at 4.67 and 8.30 ppm, respectively, gave a ratio of 0.97/0.03, which indicated the formation of α -AN with 97% efficiency with only 3% imine product. Notably, aromatic protons of the parent polymer shifted upfield after the reaction and were observed at 7.06 - 7.44 ppm overlapped with aromatic protons of the formed α -AN and imine products. The structure of P1 was further confirmed by the FT-IR spectrum given in Fig. 2C. Aldehyde C=O stretching peak at 1698 cm⁻¹ disappeared while a broad peak at 3300 cm⁻¹ assignable to the formed NH group was observed. The molecular weight (*M_w*) of P1 was also measured by GPC and found to be higher than P0 as expected, precisely 200 kDa, and its *Đ* was 2.64.

The proposed strategy was also extended to a range of amine compounds, from short and long-chain aliphatic amines to allylamine and cyclohexylamine. The results of the amine scope are collected in Table 4.

Table 4 Amine scope of the reaction^a

Polymer	Amine	<i>M_w</i> (kDa) ^b / <i>Đ</i> ^b	Efficiency (%) ^c
P0		100.0/2.33	-
P1	benzylamine	200.0/2.64	97/3/0
P2	propylamine	150.8/4.37	90/8/2
P3	butylamine	170.7/3.03	90/10/0
P4	pentylamine	220.4/2.19	90/10/0
P5	hexylamine	130.9/2.24	90/10/0
P6	dodecylamine	190.8/3.19	75/18/7
P7	allylamine	180.9/4.23	85/6/9
P8	cyclohexylamine	160.3/3.36	27/66/7

^aReactions were carried out using amine/TMSCN/*p*-TsOH at a mole

ratio of 2/1.5/0.1 per repeating unit of P0 in 1 mL of THF at room temperature for 2 h. ^bDetermined by GPC calibrated based on linear PS standards in THF. ^cMole ratios of α -aminonitrile/imine/aldehyde segments in the resulting polymer were determined by ¹H NMR.

For all amine compounds, the M_w of the modified polymer was higher than P0, and α -AN efficiency was between 27% and 97%. When aliphatic amines with shorter alkyl chains were used, the conversion of aldehyde to α -AN was 90% (Table 4, entries 2-5), while dodecylamine gave 75% efficiency for α -AN formation (Table 4, entry 6). Allylamine

also showed good efficiency with 85% α -AN and 6% imine products (Table 4, entry 7). Lastly, in the case of cyclohexylamine, the predominant product was imine with 66% efficiency, while only 27% α -AN was obtained, and 7% of aldehyde remained unreacted (Table 4, entry 8), which can be attributed to the steric hindrance of the bulky cyclohexyl group. ¹H NMR spectra of selected modified polymers are given in Fig. 3, showing distinct signals related to their chemical structure and thus confirming the attachment of these groups to P0.

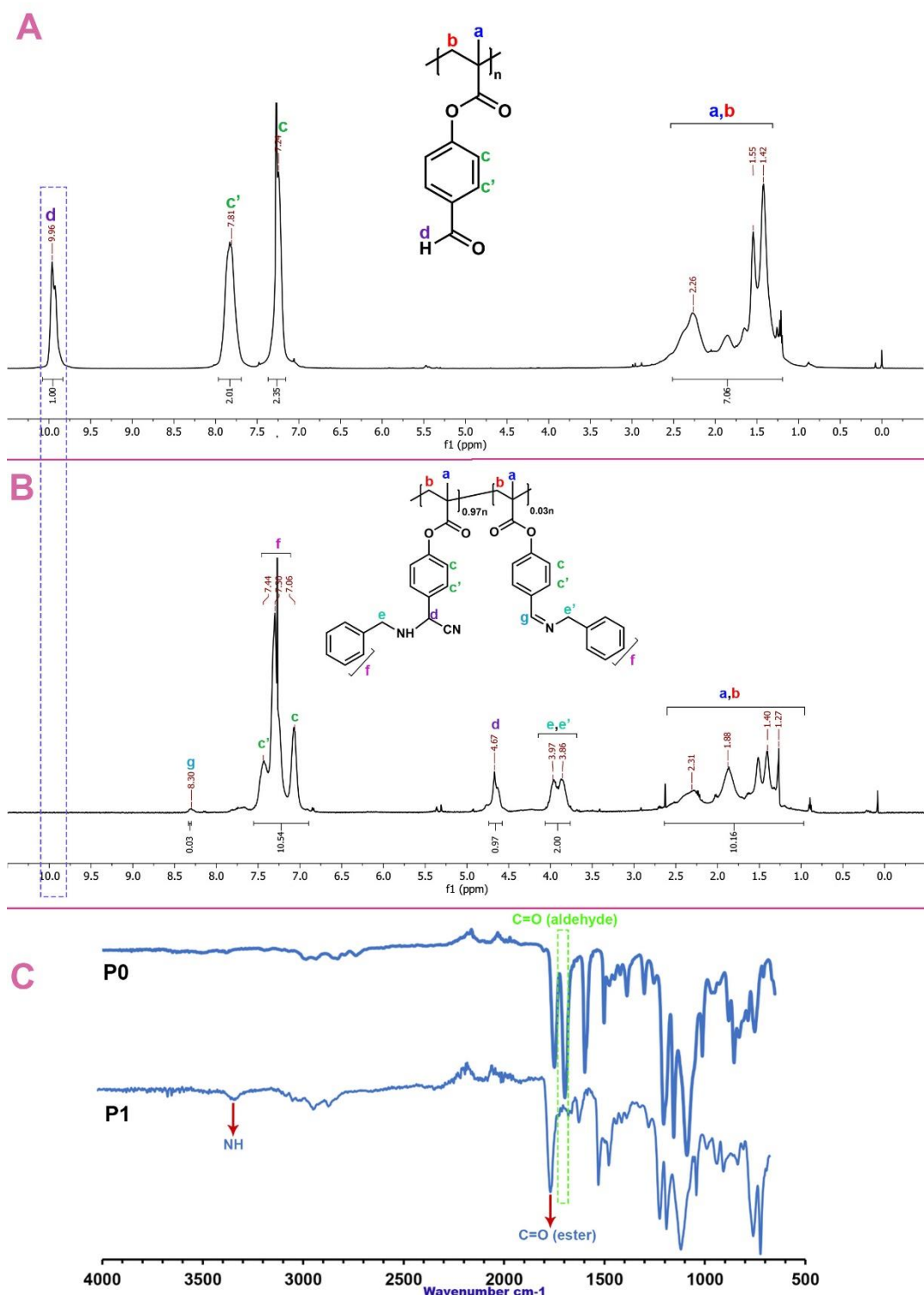


Fig. 2. ¹H NMR (A and B) and FT-IR spectra (C) of P0 and P1.

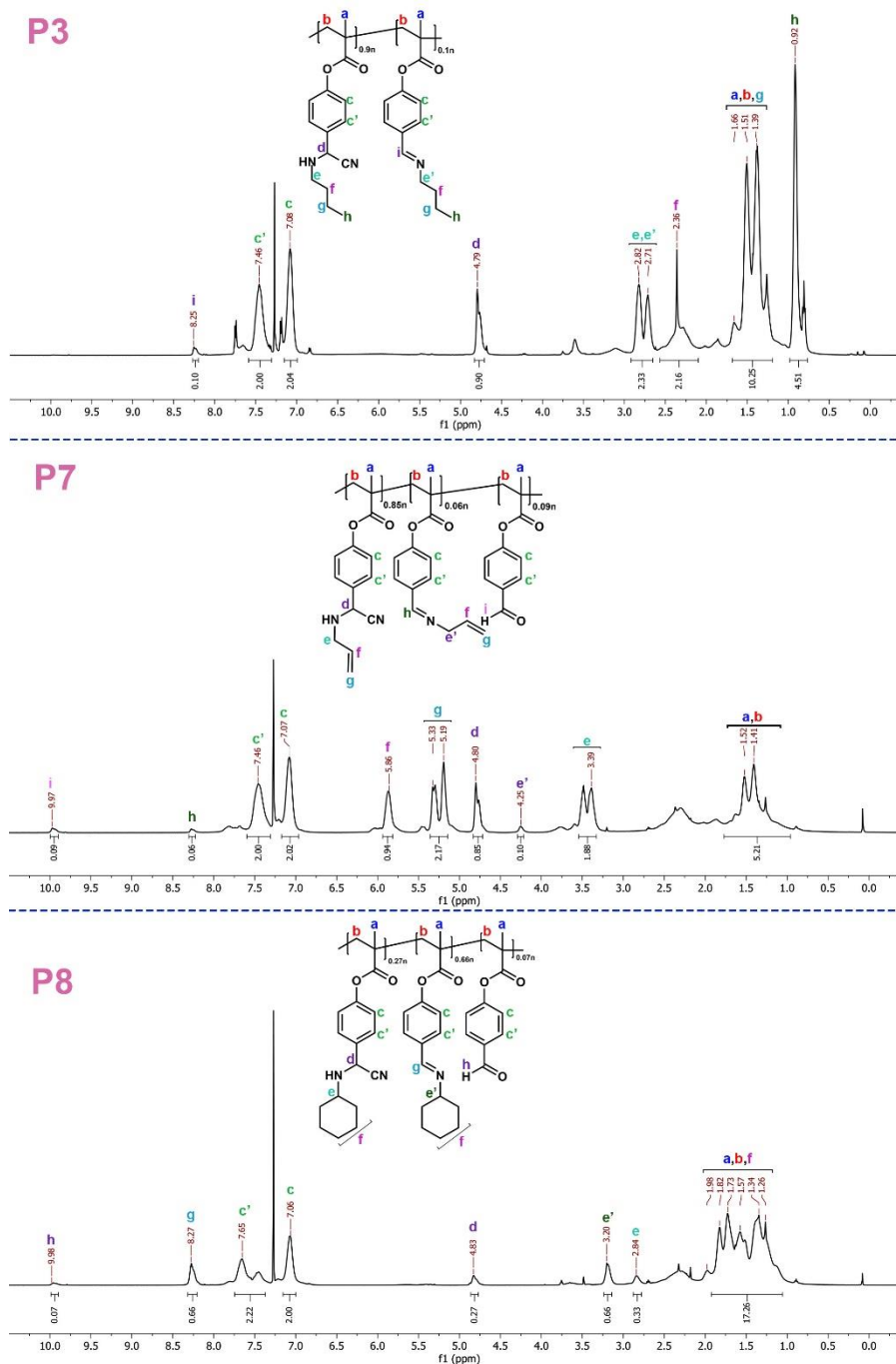


Fig. 3. ¹H NMR spectra of P3, P7 and P8.

4. Conclusion

In summary, the versatility of aldehydes was successfully extended for the first time to the Strecker 3-component reaction (S-3CR) for PPM of aldehyde-functional polymers using different amine compounds and trimethylsilyl cyanide. It was found that pendant aldehyde can be converted to α-aminonitrile with moderate to near quantitative efficiencies, as confirmed by various spectroscopic analyses. Given the growing interest in MCRs, it is believed the proposed strategy might be a good candidate to study in this field as it offers operationally simple reaction conditions. Overall, this study may pave a new way for PPM in the polymer literature.

Author Contributions

The authors contributed equally to this work.

Acknowledgements



This work was supported by the Research Fund of the Istanbul Technical University (Project Number: PTA-2022-43987).

References

- Akar, E., Kandemir, D., Luleburgaz, S., Kumbaraci, V., & Durmaz, H. (2022). Efficient Post-Polymerization modification of pendant aldehyde functional polymer via reductive etherification reaction. *European Polymer Journal*, 177, 111440. <https://doi.org/10.1016/j.eurpolymj.2022.111440>.
- Blasco, E., Sims, M.B., Goldmann, A.S., Sumerlin, B.S., & Barner-Kowollik, C. (2017). 50th Anniversary perspective: Polymer functionalization *Macromolecules*, 50 (14), 5215-5252. [10.1021/acs.macromol.7b00465](https://doi.org/10.1021/acs.macromol.7b00465).

- Cioc, R.C., Ruijter, E. & Orru, R.V.A. (2014). Multicomponent reactions: advanced tools for sustainable organic synthesis, *Green Chem.*, 16, 2958-2975. <https://doi.org/10.1039/C4GC00013G>.
- Gao, Y., & Lam, Y. (2008). Polymer-Supported N-Phenylsulfonyloxaziridine (Davis Reagent): A Versatile Oxidant. *Advanced Synthesis & Catalysis*, 350(18), 2937-2946. <https://doi.org/10.1002/adsc.200800500>.
- García-Acosta, B., García, F., García, J. M., Martínez-Máñez, R., Sancenón, F., San-José, N., & Soto, J. (2007). Chromogenic signaling of hydrogen carbonate anion with pyrylium-containing polymers. *Organic Letters*, 9(13), 2429-2432. <https://doi.org/10.1021/ol0705191>.
- Geng, Z., Shin, J.J., Xi, Y., & Hawker, C.J. (2021). Click chemistry strategies for the accelerated synthesis of functional macromolecules *J. of Polym. Sci.*, 59 (11), 963-1042. [10.1002/pol.20210126](https://doi.org/10.1002/pol.20210126).
- Günay, K.A., Theato, P., & Klok, H.A. (2013). Standing on the shoulders of Hermann Staudinger: Post-polymerization modification from past to present *J. Polym. Sci., Part A: Polym. Chem.*, 51 (1), 1-28. [10.1002/pola.26333](https://doi.org/10.1002/pola.26333).
- Harusawa, S., & Shioiri, T. (2016). Diethyl phosphorocyanidate (DEPC): a versatile reagent for organic synthesis. *Tetrahedron*, 72(50), 8125-8200. <https://doi.org/10.1016/j.tet.2016.09.070>.
- Ishitani, H., Komiya, S., & Kobayashi, S. (1998). Catalytic, Enantioselective Synthesis of α -Aminonitriles with a Novel Zirconium Catalyst. *Angewandte Chemie International Edition*, 37(22), 3186-3188. [https://doi.org/10.1002/\(SICI\)1521-3773\(19981204\)37:22%3C3186::AID-ANIE3186%3E3.0.CO;2-E](https://doi.org/10.1002/(SICI)1521-3773(19981204)37:22%3C3186::AID-ANIE3186%3E3.0.CO;2-E).
- Jackson, A. W., Stakes, C., & Fulton, D. A. (2011). The formation of core cross-linked star polymer and nanogel assemblies facilitated by the formation of dynamic covalent imine bonds. *Polymer Chemistry*, 2(11), 2500-2511. <https://doi.org/10.1039/C1PY00261A>
- Kim, J. S., Yoo, S. W., Kim, J. A., & Kim, J. H. (2012). Covalently assembled bifunctional copolymer layers as a matrix for immobilization of oligonucleotides. *Bulletin of the Korean Chemical Society*, 33(4), 1401-1404. <http://dx.doi.org/10.5012/bkcs.2012.33.4.1401>.
- Kouznetsov, V.V., & Galvis, C.E.P. (2018). Strecker reaction and α -amino nitriles: Recent advances in their chemistry, synthesis, and biological properties. *Tetrahedron*, 74(8), 773-810. <https://doi.org/10.1016/j.tet.2018.01.005>.
- Kreye, O., Tóth, T., & Meier, M. A. (2011). Introducing multicomponent reactions to polymer science: Passerini reactions of renewable monomers. *Journal of the American Chemical Society*, 133(6), 1790-1792. <https://doi.org/10.1021/ja1113003>.
- Kusumoto, S., Ito, S., & Nozaki, K. (2013). Direct aldol polymerization of acetaldehyde with organocatalyst/Brønsted acid systems. *Asian Journal of Organic Chemistry*, 2(11), 977-982. <https://doi.org/10.1002/ajoc.201300134>.
- Liu, Y., Zhang, J., Zhang, J., Pei, H., Liu, X., Jin, H., ... & Zhang, L. (2023). Strecker Reactions of Formaldehyde with TMSN, Catalyzed by TBAF and Formic Acid: N-Monocyanomethylation of Primary Amines. *Advanced Synthesis & Catalysis*, 365(1), 2-7. <https://doi.org/10.1002/adsc.202200767>.
- Maleki, A., Akhlaghi, E., & Paydar, R. (2016). Design, synthesis, characterization and catalytic performance of a new cellulose-based magnetic nanocomposite in the one-pot three-component synthesis of α -aminonitriles. *Applied Organometallic Chemistry*, 30(6), 382-386. <https://doi.org/10.1002/aoc.3443>.
- Nakamura, S., Sato, N., Sugimoto, M., & Toru, T. (2004). A new approach to enantioselective cyanation of imines with Et₂AlCN. *Tetrahedron: Asymmetry*, 15(9), 1513-1516. <https://doi.org/10.1016/j.tetasy.2004.03.040>.
- Negrell, C., Voirin, C., Boutevin, B., Ladmiral, V., & Caillol, S. (2018). From monomer synthesis to polymers with pendant aldehyde groups. *European Polymer Journal*, 109, 544-563. <https://doi.org/10.1016/j.eurpolymj.2018.10.039>.
- Ranu, B. C., Dey, S. S., & Hajra, A. (2002). Indium trichloride catalyzed one-step synthesis of α -amino nitriles by a three-component condensation of carbonyl compounds, amines and potassium cyanide. *Tetrahedron*, 58(13), 2529-2532. [https://doi.org/10.1016/S0040-4020\(02\)00132-1](https://doi.org/10.1016/S0040-4020(02)00132-1).
- Ravi Sankar, T., Abdul Ravoof, S. K., Kesavulu, K., & Venkata Ramana, P. (2008). Synthesis, Characterization and Thermal Studies of Polymer-Metal Complexes Derived from Poly (4-Methacryloxybenzaldehyde)-Divinylbenzene Benzoyl Hydrazone Resins. *Designed monomers and polymers*, 11(5), 457-471. <https://doi.org/10.1163/156855508X328158>.
- Reddy, C. S., & Raghu, M. (2008). *p*-Toluenesulfonic acid catalyzed rapid and efficient protocol for one-pot synthesis of α -amino nitriles. *Indian Journal of Chemistry - Section B Organic and Medicinal Chemistry*, 47(10), 1572-1577.
- Shen, K., Liu, X., Cai, Y., Lin, L., & Feng, X. (2009). Facile and efficient enantioselective strecker reaction of ketimines by chiral sodium phosphate. *Chemistry-A European Journal*, 15(24), 6008-6014. <https://doi.org/10.1002/chem.200900210>.
- Sipos, S., & Jablonkai, I. (2009). One-pot synthesis of α -aminonitriles from alkyl and aryl cyanides: a Strecker reaction via aldimine alanes. *Tetrahedron Letters*, 50(16), 1844-1846. <https://doi.org/10.1016/j.tetlet.2009.02.004>.
- Strecker, A. (1850). Ueber die künstliche Bildung der Milchsäure und einen neuen, dem Glycocol homologen Körper. *Justus Liebigs Annalen der Chemie*, 75(1), 27-45. <https://doi.org/10.1002/jlac.18500750103>.
- Suematsu, K., Nakamura, K., & Takeda, J. (1983). Polyimine, a C=N double bond containing polymers: synthesis and properties. *Polymer Journal*, 15(1), 71-79. <https://doi.org/10.1295/polymj.15.71>.
- Tunca, U. (2018). Click and multicomponent reactions work together for polymer chemistry. *Macromolecular Chemistry and Physics*, 219(16), 1800163. <https://doi.org/10.1002/macp.201800163>.
- Xi, M., Duan, C., Chi, J., Fu, T., Su, X., & Wang, H. An Efficient and Rapid Synthesis of α -Aminonitriles via Strecker Reaction Catalyzed by Humic Acid. *Chinese Journal of Organic Chemistry*, 202301024. <https://doi.org/10.6023/cjoc202301024>.
- Zhi, S., Ma, X., & Zhang, W. (2019). Consecutive multicomponent reactions for the synthesis of complex molecules. *Organic & Biomolecular Chemistry*, 17(33), 7632-7650. <https://doi.org/10.1039/C9OB00772E>.

Perspectives on the Curing of Benzoxazine Resins

Barış Kışkan^{1*} , Füsün Şeyma Güngör¹ 

¹Istanbul Technical University, Department of Chemistry, 34469, Maslak, Istanbul, Turkey

Abstract:

Benzoxazines are a class of heterocyclic compounds that can be polymerized to form polybenzoxazines, which have excellent properties such as thermal stability, flame retardance, low shrinkage, and chemical resistance. The curing of benzoxazines involves a thermal cationic ring-opening polymerization, which can be influenced by various factors such as catalysts, co-monomers, temperature, and time. In general, the curing temperatures of benzoxazines are considered as high and lie between 180 °C and 260 °C depending on the monomer structure. This nature of benzoxazine resins could limit their wider applications in different areas. Therefore, lowering the curing temperatures could play a critical role in the benzoxazine resin chemistry. This review summarizes the recent advances in the understanding of the curing mechanisms of benzoxazine resins, with a focus on the factors influencing the curing kinetics and the resulting material properties.

Keywords: Benzoxazines, polybenzoxazine, ring-opening polymerization, catalysis

Benzoksazin Reçinlerinin Kûrlenmesi Üzerine Perspektif

Özet:

Benzokazinler, bir heterosiklik bileşik sınıfıdır ve polimerleştirilerek polibenzoksazinlere dönüştürülebilirler. Polibenzokazinlerin genel özellikleri sırasıyla termal kararlılık, alev geciktirme, oluşumları sırasında boyutsal kararlılık ve kimyasallara, asit ve bazlara karşı yüksek gösterirler. Benzokazinlerin kûrlenmeleri, çeşitli faktörler tarafından etkilenebilen termal olarak tetiklene ve sürdürülen katyonik halka açılım polimerizasyonunu şekillendirir. Bu faktörler arasında katalizörler, ko-monomerler, sıcaklık ve kûrlenme zamanı bulunmaktadır. Genel olarak, benzokazinlerin kûrlenme sıcaklıkları yüksek olarak kabul edilir ve monomerin yapısına bağlı olarak 180 °C ile 260 °C arasında değişir. Benzokazin reçinelerinin bu doğası, farklı alanlarda daha geniş uygulamalarını sınırlandırabilir. Bu nedenle, kûrleme sıcaklıklarını düşürmek, benzokazin reçine kimyasında kritik bir rol oynayabilir. Bu derleme, benzokazin reçinelerinin kûrlenme mekanizmalarının anlaşılmasında son zamanlardaki ilerlemeleri, kûrlenme kinetiğini etkileyen faktörleri ve ortaya çıkan malzeme özelliklerini özetlemektedir.

Anahtar Kelimeler: Benzoksazin, polibenzoksazin, halka açılma polimerizasyonu, kataliz

REVIEW

Corresponding Author: Baris Kiskan, kiskanb@itu.edu.tr

Citation: Baris Kiskan, Fusun Seyma Gungor (2023), Perspectives on the Curing of Benzoxazine Resins, ITU ARI Bulletin of the Istanbul Technical University 2024,55 (2) 37–44.

Submission Date : 17 December 2023

Online Acceptance : 24 February 2024

Online Publishing : 24 February 2024

1. Introduction

Classical phenolic resins, namely phenol-formaldehyde resins, have maintained a continuous interest in the industry since their first production at the beginning of the 1900s. Especially, phenolic resins are still widely preferred for commodity production, construction, and even for high-tech materials, due to their noteworthy features. These properties can be given shortly as good mechanical and thermal performance, resistance to various chemicals, acids, and bases. Additionally, they exhibit good performance under fire, and emit relatively low amounts of smoke,

when exposed to flames. Therefore, phenolic resins can compete with systems based on epoxy in thermo-structural applications within the aerospace industry. Phenolic resins such as Novolac and Resol are the second dominant polymer class, after epoxy resins when fundamental properties of high-performance materials are considered for applications (Kiskan & Yagci, 2020; Pilato, 2010).

Moreover, phenolic resins can be modified to enhance their properties. For example, boron-modified phenolic resins (BPF) have excellent heat resistance and ablative properties, good mechanical and wear resistance, and flame retardancy. Alternatively, lignin is a promising substitute for phenol in phenolic resin production and can be obtained from biomass. These

modified resins can be used as adhesives for wood-based products (Zakzeski et al., 2010).

On the other hand, another noteworthy phenolic system is polybenzoxazines. Particularly, these polymers are strong contenders to Novolac. Because the structure of polybenzoxazines resembles the Novolac molecular structure to a high extent. Therefore, polybenzoxazines were commercialized successfully among the hundreds of other polymers introduced in scientific literature (Ghosh et al., 2007; Nair, 2004).

As stated, polybenzoxazines share some structural units with Novolacs, thus they inherit many similar properties. However, they differ in repeat units compared to Novolacs. They contain phenolic –OH and –CH₂–NR–CH₂– bridges in close proximity (see Scheme 1). This unique structure creates inter- and intra-molecular hydrogen bonds between these groups and significantly influences the orientation of polymer chains (Ishida & Agag, 2011).

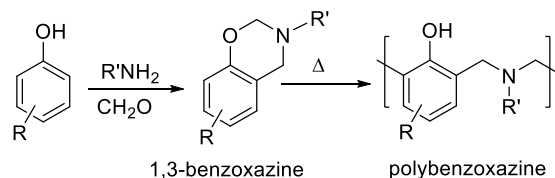
Typically, polybenzoxazines exhibit key characteristics, including minimal shrinkage during curing, high mechanical strength, a high glass transition temperature (T_g) and can reach as much as 350 °C, and a good amount of char yields above 600 °C. Additionally, these polymers exhibit chemical resistance against acids and bases similar to Novolac resins. And interestingly, polybenzoxazines differ from Novolacs extensively when compared to water absorption because polybenzoxazines display low water adsorption, as a consequence of intramolecular hydrogen bonding. The appealing properties of polybenzoxazines captured much interest from the industry and led to diverse applications of polybenzoxazines, particularly in composites, electronic circuit boards, and high-performance material production (Ishida & Agag, 2011)

The benzoxazine structure has different isomers (1,2-, 1,4-, and 3,1-), but it is known that only the 1,3-isomers could be polymerized to produce polybenzoxazines until this date. Although benzoxazines could act as monomers for polybenzoxazine production this property was unknown at the initial introduction of these molecules. (Ishida & Agag, 2011) The initial synthesis of 1,3-benzoxazines was documented in 1944. The standard method for synthesizing benzoxazines requires using one equivalent of phenol (or diphenol or multifunctional phenols), one equivalent of primary amine, and two equivalents of formaldehyde. This synthesis involves both Mannich and simultaneous ring-closure reactions. To achieve ring-closure reaction, it is essential to choose a phenol with an unoccupied ortho position. (Scheme 1) (Burke, 1949; Burke et al., 1952; Burke et al., 1954; Burke & Weatherbee, 1950; Holly & Cope, 1944).

While benzoxazines have been in the scientific spotlight since the 1940s, their early applications in the 1950s and 60s were primarily centered around exploring potential medicinal effects against tumors. Unfortunately, the 1,3-benzoxazine isomer showed limited efficacy, prompting a shift in research focus toward other oxazine isomers and oxazinones. After having more insights into the limited medicinal capacity of 1,3-benzoxazines. The research on 1,3-benzoxazine chemistry continued sluggishly until 1973 (Burke et al., 1965; Gaines & Swanson, 1971; Schreiber H, 1973).

The potential of these compounds as monomers in polymer science gained recognition in 1973 with a patent of Schreiber on the formation of oligobenzoxazines from 1,3-benzoxazines. Thereafter, the breakthrough continued in 1985 with the patenting of a thermoset based on polybenzoxazine obtained from multifunctional benzoxazines. The detailed properties of polybenzoxazines were finally revealed in 1994 by Ning and Ishida, as a significant milestone in the exploration of these compounds in polymer and material science (Higginbottom, 1985; Ning & Ishida, 1994; Schreiber H, 1973).

Subsequently, numerous reports were published about various aspects of benzoxazine polymerization, their distinctive features, curing behaviors, and more. (Ghosh et al., 2007) Notably, these studies highlighted that the polymerization of benzoxazines could be achieved by directly heating monomers to temperatures ranging from 180 to 250 °C, which is the common method without the use of catalysts, as depicted in Scheme 1. The curing temperature is a critical parameter that affects the properties of benzoxazines. Higher curing temperatures generally lead to higher crosslinking density, which results in improved mechanical and thermal properties of the cured polymers. However, excessively high curing temperatures can cause thermal degradation and adversely affect the properties of the cured polymers (Pei et al., 2021).

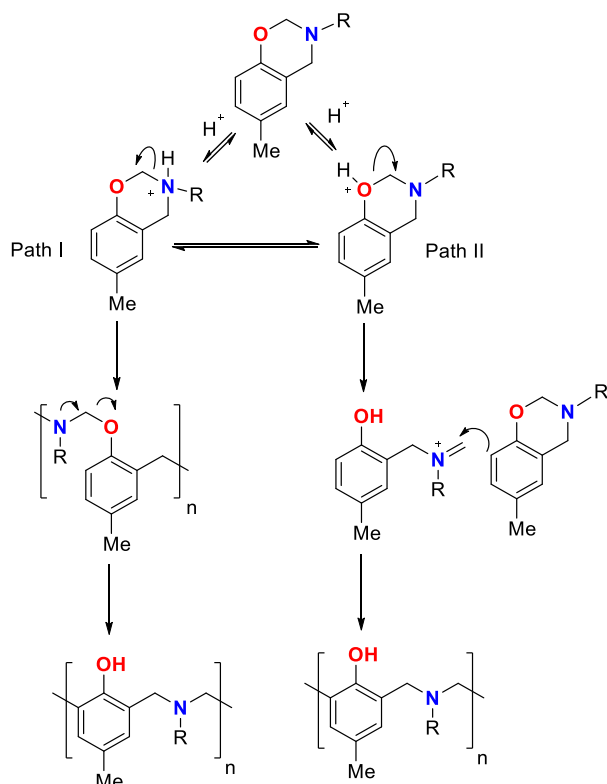


Scheme 1. Synthesis and ring-opening polymerization of 1,3-benzoxazines.

The curing behavior of benzoxazines is affected by several factors, such as the structure and reactivity of the monomers, the presence and type of catalysts, the ratio and compatibility of co-monomers, the curing temperature and time, and the degree of conversion. These factors can influence the kinetics, thermodynamics, gelation, network formation, and properties of the cured polybenzoxazines. Therefore, it is important to understand the curing process of benzoxazines to optimize their performance and applications (Jubsilp et al., 2006; Kim et al., 1999).

According to mechanistic studies, a general consensus developed on the major pathways of curing reactions of benzoxazines. Accordingly, the polymerization of benzoxazines occurs via a cationic pathway initiated by the reaction of the residual phenolic –OH groups of the monomers. This process can be summarized as follows; Protonation: There are two protonation possibilities, either on the N or O atom, leading to two different routes for the initiation of polymerization. Initiation: The protonated N and O atoms present on the oxazine ring form relatively stabilized cations, and then ring-opening takes place. Propagation: After the formation of cationic intermediates an electrophilic aromatic substitution or etherification over phenolic oxygen takes place to form benzoxazine dimer. Then, the repetitions of the abovementioned reactions create polybenzoxazine. Although the initiation site affects the intermediates and creates different pathways for ring-opening polymerization the final polymer structure is considered to be the same for all pathways because the aryl ether structure undergoes a rearrangement reaction to form polybenzoxazine (Scheme 2). However, there are some restrictions to consider such as high curing temperatures. The polymerization of benzoxazines does not require additional catalysts or curative, but high curing temperatures are a limitation. Because high temperatures result in high amount of energy consumption and degrade the thermally susceptible functional groups on polybenzoxazines (Chutayothin & Ishida, 2010; Furuncuoğlu Özalpın et al., 2018; Hamerton et al., 2013; Kasapoglu et al., 2003; Urbaniak et al., 2017; Wang et al., 2020).

Therefore, lower ring-opening polymerization (ROP) temperatures would be significant. This perspective article summarizes the major strategies that are used to overcome the high ring opening polymerization temperatures of benzoxazines. And provides insights into the polymerization part of the benzoxazine chemistry.



Scheme 2. The summarized mechanism for ring-opening polymerization of a typical benzoxazine

2. Major Strategies to Reduce the Cure Temperature of Benzoxazines

The polymerization of benzoxazines is a complex process involving cationic initiation, protonation, and ring-opening. Lower ROP temperatures would be beneficial for energy economy and to prevent thermally susceptible functional groups on polybenzoxazines from degradation. Further research is needed to develop methods for reducing the curing temperature and optimizing the polymerization process.

To reduce the high curing temperatures required for the ring-opening polymerization (ROP) of benzoxazines, various catalysts have been employed, including organic or Lewis acids and compounds with nucleophilic character. For example, PCl_5 , POCl_3 , AlCl_3 , TiCl_4 , and FeCl_3 with suitable solvents have been shown to have good catalytic activities. The use of a mixture of a Lewis acid and a nucleophilic catalyst has also been found to be effective in promoting the polymerization, with acetylacetonato complexes of transition metals of the 4th period acting as highly efficient catalysts. However, these active catalysts often initiate ROP of benzoxazines at room temperature and can increase the viscosity of benzoxazine based formulations significantly prior to usage and during storage. Therefore, these catalyst administrations can reduce the shelf life of benzoxazine formulations in practical use. To overcome this problem, latent catalysts that are dormant at room temperature or certain temperatures but generate active initiators by heating have been developed. For example, diamines, thiols, elemental sulfur and toluene sulfonates have been successfully used to reduce ROP temperatures for classical mono- and di-functional benzoxazines.

Specially designed benzoxazine monomers with free phenolic -OH groups or naphthoxazines have also been found to reduce the ROP temperature to certain values. In conclusion, various catalysts have been employed to reduce the high curing temperatures required for the ROP of benzoxazines. While admixed catalysts can initiate ROP at room temperature, latent catalysts that generate active initiators by heating have been

developed to overcome this problem. Further research is needed to optimize the polymerization process and reduce the curing temperature of benzoxazines. Accordingly, this manuscript discusses the major strategies to reduce the cure temperature of benzoxazines (Akkus et al., 2019, 2020; Coban et al., 2021; Deliballi et al., 2021; Espinosa et al., 2003; Kaya et al., 2018; Kocaarslan et al., 2017; Kudoh et al., 2010; Liu et al., 2013; Liu, Shen, Sebastián, et al., 2011; Lochab et al., 2021; Oie et al., 2010; Sudo et al., 2010)

2.1 Acid Catalyzed Systems

Acidic initiators are commonly preferred for their commercial availability and different acidic strengths, which makes them good candidate to mediate cationic ring-opening polymerization (ROP) of benzoxazines. These acid initiators can protonate oxygen or the nitrogen atom of the oxazine ring, facilitating the formation of intermediate iminium ions (see Scheme 2). The protonation of nitrogen atom resulting an iminium ion intermediate, which is relatively a stable cationic species. Consecutive electrophilic reactions result in O-attack, N-attack, and aryl-attack on the benzoxazine monomer which then led to the growth of the polymer. Due to the N and O attacks the polymer may contain phenoxy and phenolic linkages. When ortho-positions are obstructed either by a steric hindrance or a functional group the polymerization is anticipated to take place at an accessible para-position to the benzoxazine ring. In summary, acidic initiators play a crucial role in mediating the cationic ROP of benzoxazines by protonating the oxygen or nitrogen atom of the oxazine ring, leading to the formation of stable iminium ion intermediates and subsequent polymer growth. This mechanism is essential for understanding the polymerization process and optimizing the synthesis of benzoxazine-based polymers (Andreu et al., 2008; Dunkers & Ishida, 1999; Kim & Ishida, 2001; Yagci et al., 2009; Zúñiga et al., 2011).

Ishida *et al.* (Ishida & Rodriguez, 1995) examined the utilization of phenols possessing an unoccupied ortho-position, such as butylated hydroxyanisole (BA), poly(*p*-hydroxystyrene), 2,2'-dihydroxybenzophenone, and 2,6-di-*tert*-butyl-*p*-cresol. They also investigated both mild and strong organic and mineral acids, including acetic, adipic, benzoic, sebacic, sulfuric, *p*-toluenesulfonic, and phosphoric acids, as catalysts for the ring-opening polymerization of the benzoxazine monomer. Among these, adipic acid at 6 mol% was found to be the most effective catalyst, demonstrating a significant 17% decrease in the curing temperature.

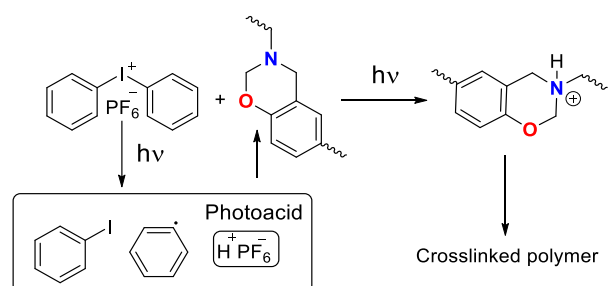
Interestingly, polybenzoxazines (PBZs) produced with strong carboxylic acids exhibited inferior properties compared to those formed with weak carboxylic acids. The acidity level, as indicated by the pKa of the acid, was identified as a crucial factor controlling the conversion of the intermediates, thereby influencing crosslinking of the system. The characteristic IR vibrations of oxazine ring at 1050 and 813 cm^{-1} exhibited a more rapid decrease in the presence of *p*-cresol (pKa = 10.2) compared to sebacic acid (pKa = 4.7, 5.4), supporting the notion that *p*-cresol mediates a faster oxazine ring-opening reaction.

Ishida and colleagues (Ishida & Rodriguez, 1995) provided more insights into the impact of phenols on the polymerization reaction and its associated pathways by investigating the reaction between 2,4-xyleneol and 3-aryl substituted benzoxazine. This investigation revealed the formation of various inter- and intra-molecular rearranged products as intermediate species. Notably, Bisphenol F was found to be a more effective catalyst than BA, possibly due to the distinct electron-donating capabilities of the methylene versus isopropylidene bridge in biphenols. Furthermore, a substantial loading (~40 wt%) of cashew nut shell liquid (CNSL, contains phenolic compounds) in bisphenol A-aniline benzoxazine led to a decrease in both peak temperature and ΔH from 216 °C

and 246 J.g⁻¹ to 197 °C and 194 J.g⁻¹, respectively. The ring opening polymerization reaction demonstrated an autocatalytic nature due to the formation of ring-opened phenolic structures after each addition of benzoxazine. For instance, resorcinol-aniline (Rc-a) benzoxazine exhibited polymerization at a much lower temperature compared to phenol-aniline (Ph-a), attributed to the formation of two phenolic –OH groups in the structure of Rc-a versus one in Ph-a. The presence of a low amount of phenols serves as an initiator, impacting the rate and temperature that are required for the successful ring-opening polymerization reaction.

Hamerton *et al.* reported that 3,3-thiodipropionic acid (TDA), with a higher pKa value (4.11), acts as a superior initiator compared to 3,3-thiodiphenol, resulting in a reduction of cure T_{onset} and a simultaneous increase in crosslink density, reflected in a higher T_g value in the resulting polymer. Additionally, renewable phenolic acids such as cinnamic, coumaric, ferulic, and phloretic acids were employed as catalysts to lower the polymerization temperature of the reaction (Hamerton *et al.*, 2013).

The use of diphenyliodonium (Ph₂I⁺PF₆⁻) and triphenylsulfonium (Ph₃S⁺PF₆⁻) salts in photoinitiated cationic polymerization has been shown to result in the light-induced formation of protons, leading to the formation of polybenzoxazine with a 72% conversion (Scheme 3). At high monomer concentrations (>0.5 mol L⁻¹), oligomer formation occurred, indicating chain transfer reactions that have negative impact on polymerization. Additionally, carbon-centered radicals generated by the photolysis of 2,2-Dimethoxy-2-phenylacetophenone (DMPA) undergo oxidation to form the corresponding carbocations, initiating the polymerization of the monomer. Despite being initially considered moderate initiators, diphenyliodonium salts (ArI⁺ X⁻) have proven highly effective as photoinitiators. In their presence, the polymerization profiles of BA-a exhibited a broader curing exotherm at 162 °C. The polymerization takes place such as the decomposition of iodonium salt and formation of H⁺X⁻, and the second step is protonation of benzoxazines and the initiation ring-opening. These findings highlight the effectiveness of diphenyliodonium and triphenylsulfonium salts as photoinitiators for cationic polymerization, with implications for the polymerization profiles and initiation activity of the photoinitiator salt (Deliballi *et al.*, 2021; Kasapoglu *et al.*, 2003).



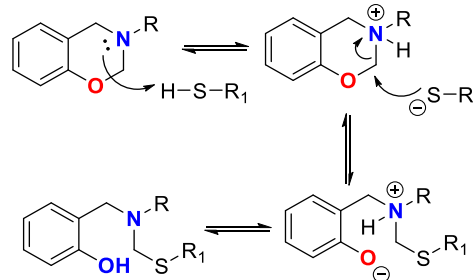
Scheme 3. Curing of benzoxazines via iodonium salt

Alternatively, cyanuric chloride (2,4,6-trichloro-1,3,5-triazine) was also used in the curing of benzoxazines. The mechanism lies on the reaction of cyanuric chloride with humidity or other nucleophiles to produce acids (HCl and cyanuric acid) *in situ* for initiating ROP of Bz (Akkus *et al.*, 2020).

Unlike phenols, thiophenols exhibit a reversible reaction with benzoxazine (Bz) monomers at room temperature, making them particularly promising for practical applications. Thiol compounds demonstrate greater efficiency at concentrations due to their hydrogen-donating capability. In 2011, Gorodisher *et al.* reported on the reaction of thiols with benzoxazines for adhesive purposes. This reaction was introduced as Catalytic Opening of the Lateral Benzoxazine Rings by Thiols (COLBERT) (Scheme 4). The initial step involves the protonation of the nitrogen atom by thiol, followed

by the attack of thiolate ion to the methylene group on -N-CH₂-O-group, facilitating the oxazine ring-opening reaction. This overall process mirrors the acid-catalyzed nucleophilic addition that triggers ring-opening reaction of benzoxazines. Due to the reversible nature of the reaction, even low concentrations of thiols have a notable impact on reducing the polymerization temperature, as evident in the DSC studies. This reduction is attributed to the continuous regeneration of the thiol and iminium ion which, catalyze the polymerization reaction (Gorodisher *et al.*, 2011; Gorodisher *et al.*, 2013; Salnikov *et al.*, 2014).

The rate-determining step of this reaction is found as the protonation of the N or O atom, which was supported by inhibitors. Moreover, mechanistic studies revealed that the reaction rate is significantly influenced by the acidity of the thiol and the nature of the solvent (protic vs. aprotic). Kawaguchi *et al.* investigated the interaction between *p*-cresol-aniline type benzoxazine (pC-a) and *p*-methoxythiophenol (pMOTPH), resulting in the formation of a ring-opened adduct. In these studies the reversible nature of the polymerization-depolymerization reaction was also shown. The yield of the adduct is observed to be higher in polar solvents unlike nonpolar solvents. This finding is attributed to the stabilization zwitterion/ammonium cation intermediates in polar solvents (Asei William Kawaguchi *et al.*, 2012; Asei W. Kawaguchi *et al.*, 2012; Kawaguchi *et al.*, 2014).



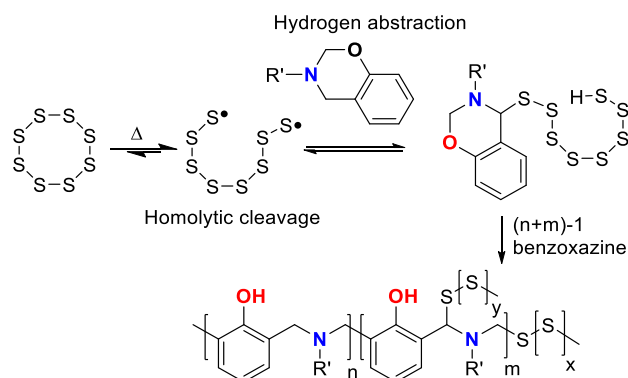
Scheme 4. Thiol initiated ROP of benzoxazines

Beyond monomers, the polymerization of main-chain type polybenzoxazine (PBz) was carried out at room temperature using different thiols, such as 1-butanethiol, 2-ethanethiol and thiophenol, in a CH₃OH/CHCl₃ solvent mixture over a 24-hour period. The successful integration of thiol compounds into PBz was validated through spectral and molecular weight characterizations (Bektas *et al.*, 2015; Beyazkilic *et al.*, 2012).

Urbaniak and colleagues proposed a mechanism wherein the reversible ring-opening of 1,3-benzoxazine with thiols occurs through an iminium ion intermediate. They suggested that the cyclic six-membered transition state had less effect on the reversible reaction. Their work clearly reveal the significance of the protonation step of benzoxazine with thiols under solvent/solvent-free conditions, wherein acidity dominates the nucleophilicity (Urbaniak *et al.*, 2017).

In addition to thiol reagents, elemental sulfur (S) has been observed to lower the polymerization temperature of benzoxazine monomer. For instance, Shukla and colleagues demonstrated a reduction in peak temperature of pC-a monomer from 263°C to 185°C in the to a copolymerization (C-a and S₈) reaction temperature. Similarly, a significant ROP temperature reduction with sulfurs was reported by Arslan *et al.* (Akay *et al.*, 2017; Arslan *et al.*, 2016; Shukla *et al.*, 2016)

The proposed mechanism suggests that generated (*in situ*) sulfur radicals react with the oxazine ring and abstract hydrogen atom from methylene linkages of oxazine. The abstracted hydrogen combines with sulfur radicals to form thiols and then thiols protonate the oxazine ring to open and then to form poly(C-a-*ran*-S) (Scheme 5). These copolymers containing sulfur have been utilized as cathodic materials in Li-S and Na-S batteries.

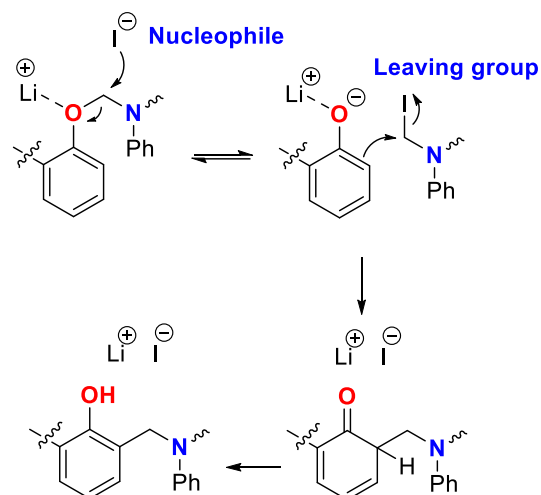


Scheme 5. Polymerization of benzoxazines via elemental sulfur

2.2. Salt and Nucleophile Catalyzed Systems

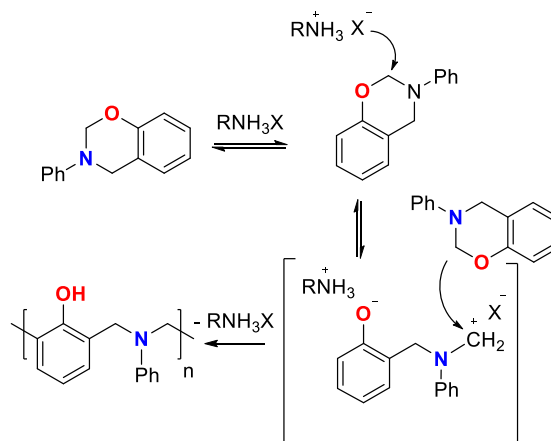
The processability and compatibility of many resins depend on the low polymerization temperature. This requirement is also valid for benzoxazine resins. One of the methods to achieve this goal is to mix Bz monomer with various salts. As well-known salts are consisted of anions and counter cations. While the cation part of the salt coordinates the oxygen atom in the oxazine ring during ring opening, the anion part acts as a nucleophile. The fact that the nucleophile is also a good leaving group accelerates the process. For this purpose, *Liu et al.* used LiI, LiBr, NaI, and LiBr/NaI salts and found that LiI was the most effective salt among these salts (*Liu, Shen, Sebastián, et al., 2011*). A mechanism for ring-opening of benzoxazines was proposed is shown in the Scheme 6.

Similarly, *Kocaarslan et al.* investigated the ROP of Bz using various amine HCl salts (NH_3OHCl , PhNH_3Cl , PhNHNH_3Cl , NH_4Cl , EtNH_3Cl) as a catalyst in 2017. As a result of the study, they found that amine HCl salts reduced the maximum ROP temperatures in e.g. from 224 °C to 185 °C (*Kocaarslan et al., 2017*).



Scheme 6. The probable mechanism of ROP of BZ in the presence of LiI.

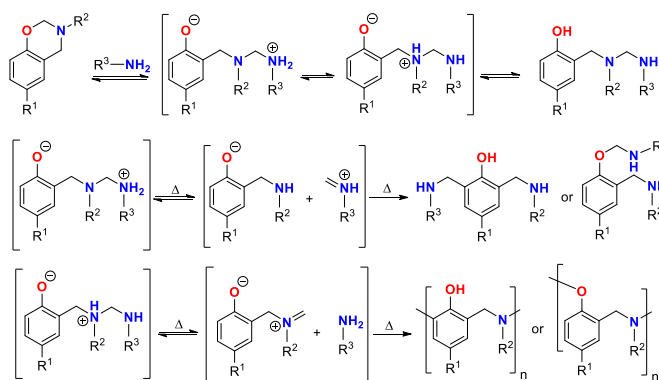
The effect of the nucleophilicity of counter ion of amine HX salts on the ROP of Bz was also studied (Scheme 7). The nucleophilicity of counter ions had shown significant effect on the ROP temperature. As nucleophilicity increases, a significant decrease in ROP temperature was observed. The general trend of reduction of ROP temperature was found to be in the order of $\text{I}^- > \text{Br}^- > \text{Cl}^-$. The study also revealed that the nucleophilic character of the counter ions, their solubility, and ionization ability of the salts in melt benzoxazine monomers had high impact on the catalytic ability (*Akkus et al., 2019*).



Scheme 7. Salt induced ROP of benzoxazines

In the study of *Agag et al.* multiple exothermic peaks were observed at low temperatures in the ROP of the amine-functional benzoxazine (*Agag et al., 2010*). Accordingly, *Sun et al.* reported a ring-opening addition reaction of benzoxazine with an amine (*Sun et al., 2015*). They suggested that polymerization occurred via a cationic mechanism (Scheme 8). In the beginning, a reversible reaction takes place between amine and benzoxazine resulting in the formation of zwitterionic intermediates with both phenolate and aminomethanaminium structures. When heated at high temperatures, aminomethanaminium generates iminium ion and these ions undergo electrophilic reactions with the aromatic ring, leading to the formation of a stable aminomethylphenols. The involvement of amines in polymerization allows the process to occur at lower temperatures (around 120 –150 °C), leading to faster reaction rates. The activation energy (E_a) for polymerization reactions follows the basicity order of amines, with arylamine being greater than alicyclic amine, which is greater than alkylamine.

Amines, such as primary, secondary, and tertiary amines, play a crucial role in facilitating the ring-opening reaction of mono-oxazine in polar solvents. This allows for crosslinking reactions to occur when diamine reacts with bis-benzoxazine at room temperature (*Zong & Ran, 2019*).



Scheme 8. ROP of benzoxazines via amine catalyst

3. Conclusion

The focus of this review is to shed light on the significance of choosing the right benzoxazine polymerization conditions when designing polybenzoxazine based materials. The structure of Bz monomers greatly impacts the formation of polymers and their subsequent applications. On the other hand, efforts to lower the polymerization temperature continue to advance, either by molecular tailoring on the benzoxazine monomers or by adding external curatives/catalysts and/or copolymerization with other polymer structures. Accordingly, in this review the use of catalysis for benzoxazine resins was

emphasized, where catalysts play a vital role in controlling polymerization and tailoring polymer properties. Moreover, this review provides insights into catalyst selection and optimization that significantly impact efficiency and kinetics benzoxazine resin polymerization. Therefore, this manuscript could elevate research and broaden polybenzoxazine scopes, particularly for low polymerization temperatures of benzoxazines where needed.

Acknowledgements

This work is dedicated to the memory of Professor Yusuf Yağcı. The authors acknowledge support from Istanbul Technical University Research Fund.

References

- Agag, T., Arza, C. R., Maurer, F. H. J., & Ishida, H. (2010). Primary Amine-Functional Benzoxazine Monomers and Their Use for Amide-Containing Monomeric Benzoxazines. *Macromolecules*, 43(6), 2748-2758. <https://doi.org/DOI: 10.1021/ma902556k>
- Akay, S., Kayan, B., Kalderis, D., Arslan, M., Yagci, Y., & Kiskan, B. (2017). Poly(benzoxazine-co-sulfur): An efficient sorbent for mercury removal from aqueous solution. *Journal of Applied Polymer Science*, 134(38), 45306-45306.
- Akkus, B., Kiskan, B., & Yagci, Y. (2019). Counterion Effect of Amine Salts on Ring-Opening Polymerization of 1,3-Benzoxazines. *Macromolecular Chemistry and Physics*, 220(1), 1800268. <https://doi.org/DOI: 10.1002/macp.201800268>
- Akkus, B., Kiskan, B., & Yagci, Y. (2020). Cyanuric Chloride as a Potent Catalyst for the Reduction of Curing Temperature of Benzoxazines [10.1039/C9PY01631G]. *Polymer Chemistry*, 11(5), 1025-1032. <https://doi.org/DOI: 10.1039/C9PY01631G>
- Andreu, R., Reina, J. A., & Ronda, J. C. (2008). Carboxylic Acid-Containing Benzoxazines as Efficient Catalysts in the Thermal Polymerization of Benzoxazines. *Journal of Polymer Science, Part A: Polymer Chemistry*, 46(18), 6091-6101. <https://doi.org/DOI: 10.1002/pola.22921>
- Arslan, M., Kiskan, B., & Yagci, Y. (2016). Combining Elemental Sulfur with Polybenzoxazines via Inverse Vulcanization. *Macromolecules*, 49(3), 767-773. <https://doi.org/DOI: 10.1021/acs.macromol.5b02791>
- Bektas, S., Kiskan, B., Orakdogan, N., & Yagci, Y. (2015). Synthesis and Properties of Organo-Gels by Thiol-Benzoxazine Chemistry. *Polymer*, 75, 44-50. <https://doi.org/DOI: 10.1016/j.polymer.2015.08.026>
- Beyazkilic, Z., Kahveci, M., Aydogan, B., Kiskan, B., & Yagci, Y. (2012). Synthesis of polybenzoxazine precursors using thiols: Simultaneous thiol-ene and ring-opening reactions. *Journal of Polymer Science Part A: Polymer Chemistry*, 50(19), 4029-4036. <https://doi.org/DOI: 10.1002/pola.26202>
- Burke, W. J. (1949). 3,4-Dihydro-1,3,2H-Benzoxazines. Reaction of p-Substituted Phenols with N,N-Dimethylolamines. *Journal of the American Chemical Society*, 71(2), 609-612. <https://doi.org/DOI:10.1021/ja01170a063>
- Burke, W. J., Bishop, J. L., Glennie, E. L. M., & Bauer, W. N. (1965). A New Aminoalkylation Reaction. Condensation of Phenols with Dihydro-1,3-oxazines. *The Journal of Organic Chemistry*, 30(10), 3423-3427. <https://doi.org/10.1021/jo01021a037>
- Burke, W. J., Kolbezen, M. J., & Stephens, C. W. (1952). Condensation of Naphthols with Formaldehyde and Primary Amines. *Journal of the American Chemical Society*, 74(14), 3601-3605. http://pubs3.acs.org/acs/journals/doi/lookup?in_doi=10.1021/ja01134a039
- Burke, W. J., Murdock, K. C., & Ec, G. (1954). Condensation of Hydroxyaromatic Compounds with Formaldehyde and Primary Aromatic Amines. *Journal of the American Chemical Society*, 76(6), 1677-1679. <https://doi.org/10.1021/ja01635a065>
- Burke, W. J., & Weatherbee, C. (1950). 3,4-Dihydro-1,3,2H-Benzoxazines. Reaction of Polyhydroxybenzenes with N-Methylolamines. *Journal of the American Chemical Society*, 72(10), 4691-4694. http://pubs3.acs.org/acs/journals/doi/lookup?in_doi=10.1021/ja01166a094
- Chutayothin, P., & Ishida, H. (2010). Cationic Ring-Opening Polymerization of 1,3-Benzoxazines: Mechanistic Study Using Model Compounds. *Macromolecules*, 43(10), 4562-4572. <https://doi.org/DOI: 10.1021/ma901743h>
- Coban, Z. G., Yagci, Y., & Kiskan, B. (2021). Catalyzing the Ring-Opening Polymerization of 1,3-Benzoxazines via Thioamide from Renewable Sources. *ACS Applied Polymer Materials*, 3(8), 4203-4212. <https://doi.org/10.1021/acsapm.1c00637>
- Deliballi, Z., Kiskan, B., & Yagci, Y. (2021). Light induced crosslinking of main chain polybenzoxazines [10.1039/D1PY01080H]. *Polymer Chemistry*, 12(40), 5781-5786. <https://doi.org/10.1039/D1PY01080H>
- Dunkers, J., & Ishida, H. (1999). Reaction of Benzoxazine-Based Phenolic Resins with Strong and Weak Carboxylic Acids and Phenols as Catalysts. *Journal of Polymer Science, Part A: Polymer Chemistry*, 37(13), 1913-1921. [https://doi.org/DOI: 10.1002/\(SICI\)1099-0518\(19990701\)37:13<1913::AID-POLA4>3.0.CO;2-E](https://doi.org/DOI: 10.1002/(SICI)1099-0518(19990701)37:13<1913::AID-POLA4>3.0.CO;2-E)
- Espinosa, M. A., Cádiz, V., & Galià, M. (2003). Synthesis and characterization of benzoxazine-based phenolic resins: Crosslinking study. *Journal of Applied Polymer Science*, 90(2), 470-481. <https://doi.org/https://doi.org/10.1002/app.12678>
- Furuncuoğlu Özeltin, T., Catak, S., Kiskan, B., Yagci, Y., & Aviyente, V. (2018). Rationalizing the regioselectivity of cationic ring-opening polymerization of benzoxazines. *European Polymer Journal*, 105, 61-67. <https://doi.org/https://doi.org/10.1016/j.eurpolymj.2018.05.024>
- Gaines, J. R., & Swanson, A. W. (1971). Preparation of 3,4-dihydro-2H-1,3-benzoxazines. *Journal of Heterocyclic Chemistry*, 8(2), 249-251. <https://doi.org/doi:10.1002/jhet.5570080212>
- Ghosh, N., Kiskan, B., & Yagci, Y. (2007). Polybenzoxazines—New High Performance Thermosetting Resins: Synthesis and Properties. *Progress in Polymer Science*, 32(11), 1344-1391. <https://doi.org/DOI: 10.1016/j.progpolymsci.2007.07.002>
- Gorodisher, I., DeVoe, R. J., & Webb, R. J. (2011). Chapter 11 - Catalytic Opening of Lateral Benzoxazine Rings by Thiols A2. In T. Agag & H. Ishida (Eds.), *Handbook of Benzoxazine Resins* (pp. 211-234). Elsevier. <https://doi.org/DOI: 10.1016/B978-0-444-53790-4.00056-4>
- Gorodisher, I., Webb, R. J., & DeVoe, R. J. (2013). *Benzoxazine-Thiol Adducts* US 8383706 B2. <https://www.google.com/patents/US8389758>
- Hamerton, I., McNamara, L. T., Howlin, B. J., Smith, P. A., Cross, P., & Ward, S. (2013). Examining the Initiation of the Polymerization Mechanism and Network Development in Aromatic Polybenzoxazines.

- Macromolecules, 46(13), 5117-5132. <https://doi.org/DOI: 10.1021/ma401014h>
- Higginbottom, H. P. (1985). *Polymerizable compositions comprising polyamines and poly(dihydrobenzoxazines)* US Pat. 4501864A). <http://www.google.com/patents/US4501864>
- Holly, F. W., & Cope, A. C. (1944). Condensation Products of Aldehydes and Ketones with o-Aminobenzyl Alcohol and o-Hydroxybenzylamine. *Journal of the American Chemical Society*, 66(11), 1875-1879. <https://doi.org/10.1021/ja01239a022>
- Ishida, H., & Agag, T. (2011). *Handbook of Benzoxazine Resins* [Book]. Elsevier. <https://doi.org/DOI: 10.1016/C2010-0-66598-9>
- Ishida, H., & Rodriguez, Y. (1995). Catalyzing the Curing Reaction of a New Benzoxazine-Based Phenolic Resin. *Journal of Applied Polymer Science*, 58(10), 1751-1760. <Go to ISI>://A1995TE63800013
- Jubsilp, C., Damrongsakkul, S., Takeichi, T., & Rimdusit, S. (2006). Curing kinetics of arylamine-based polyfunctional benzoxazine resins by dynamic differential scanning calorimetry. *Thermochimica Acta*, 447(2), 131-140. <https://doi.org/https://doi.org/10.1016/j.tca.2006.05.008>
- Kasapoglu, F., Cianga, I., Yagci, Y., & Takeichi, T. (2003). Photoinitiated cationic polymerization of monofunctional benzoxazine. *Journal of Polymer Science Part A: Polymer Chemistry*, 41(21), 3320-3328. <https://doi.org/https://doi.org/10.1002/pola.10913>
- Kawaguchi, A. W., Sudo, A., & Endo, T. (2012). Polymerization-Depolymerization System Based on Reversible Addition-Dissociation Reaction of 1,3-Benzoxazine with Thiol. *ACS Macro Letters*, 2(1), 1-4. <https://doi.org/DOI: 10.1021/mz3005296>
- Kawaguchi, A. W., Sudo, A., & Endo, T. (2012). Synthesis of Highly Polymerizable 1,3-Benzoxazine Assisted by Phenyl Thio Ether and Hydroxyl Moieties. *Journal of Polymer Science, Part A: Polymer Chemistry*, 50(8), 1457-1461. <https://doi.org/DOI: 10.1002/pola.25923>
- Kawaguchi, A. W., Sudo, A., & Endo, T. (2014). Thiol-functionalized 1,3-benzoxazine: Preparation and its use as a precursor for highly polymerizable benzoxazine monomers bearing sulfide moiety. *Journal of Polymer Science Part A: Polymer Chemistry*, 52(10), 1448-1457. <https://doi.org/https://doi.org/10.1002/pola.27131>
- Kaya, G., Kiskan, B., & Yagci, Y. (2018). Phenolic Naphthoxazines as Curing Promoters for Benzoxazines. *Macromolecules*, 51(5), 1688-1695. <https://doi.org/DOI: 10.1021/acs.macromol.8b00218>
- Kim, H. D., & Ishida, H. (2001). Study on the chemical stability of benzoxazine-based phenolic resins in carboxylic acids. *Journal of Applied Polymer Science*, 79(7), 1207-1219. <Go to ISI>://000166220400008
- Kim, H. J., Brunovska, Z., & Ishida, H. (1999). Molecular characterization of the polymerization of acetylene-functional benzoxazine resins. *Polymer*, 40(7), 1815-1822. <Go to ISI>://000078048400021
- Kiskan, B., & Yagci, Y. (2020). The Journey of Phenolics from the First Spark to Advanced Materials. *Israel Journal of Chemistry*, 60(1-2), 20-32. <https://doi.org/DOI: 10.1002/ijch.201900086>
- Kocaarslan, A., Kiskan, B., & Yagci, Y. (2017). Ammonium Salt Catalyzed Ring-Opening Polymerization of 1,3-Benzoxazines. *Polymer*, 122, 340-346. <https://doi.org/DOI: 10.1016/j.polymer.2017.06.077>
- Kudoh, R., Sudo, A., & Endo, T. (2010). A Highly Reactive Benzoxazine Monomer, 1-(2-Hydroxyethyl)-1,3-Benzoxazine: Activation of Benzoxazine by Neighboring Group Participation of Hydroxyl Group. *Macromolecules*, 43(3), 1185-1187. <https://doi.org/DOI: 10.1021/ma902416h>
- Liu, C., Shen, D., Sebastián, R. M., Marquet, J., & Schönfeld, R. (2011). Mechanistic Studies on Ring-Opening Polymerization of Benzoxazines: A Mechanistically Based Catalyst Design. *Macromolecules*, 44(12), 4616-4622. <https://doi.org/DOI: 10.1021/ma2007893>
- Liu, C., Shen, D., Sebastián, R. M., Marquet, J., & Schönfeld, R. (2013). Catalyst Effects on the Ring-Opening Polymerization of 1,3-Benzoxazine and on the Polymer Structure. *Polymer (United Kingdom)*, 54(12), 2873-2878. <https://doi.org/DOI: 10.1016/j.polymer.2013.03.063>
- Liu, C., Shen, D., Sebastián, R. M. a., Marquet, J., & Schönfeld, R. (2011). Mechanistic Studies on Ring-Opening Polymerization of Benzoxazines: A Mechanistically Based Catalyst Design. *Macromolecules*, 44(12), 4616-4622. <https://doi.org/DOI: 10.1021/ma2007893>
- Lochab, B., Monisha, M., Amarnath, N., Sharma, P., Mukherjee, S., & Ishida, H. (2021). Review on the Accelerated and Low-Temperature Polymerization of Benzoxazine Resins: Addition Polymerizable Sustainable Polymers. *Polymers*, 13(8), 1260. <https://www.mdpi.com/2073-4360/13/8/1260>
- Nair, C. P. R. (2004). Advances in Addition-Cure Phenolic Resins. *Progress in Polymer Science*, 29(5), 401-498. <https://doi.org/DOI: 10.1016/j.progpolymsci.2004.01.004>
- Ning, X., & Ishida, H. (1994). Phenolic materials via ring-opening polymerization: Synthesis and characterization of bisphenol-A based benzoxazines and their polymers. *Journal of Polymer Science Part A: Polymer Chemistry*, 32(6), 1121-1129. <https://doi.org/DOI:10.1002/pola.1994.080320614>
- Oie, H., Sudo, A., & Endo, T. (2010). Acceleration effect of N-allyl group on thermally induced ring-opening polymerization of 1,3-benzoxazine. *Journal of Polymer Science Part A: Polymer Chemistry*, 48(23), 5357-5363. <https://doi.org/10.1002/pola.24338>
- Pei, L., Zhao, S., Li, H., Zhang, X., Fan, X., Wang, W., . . . Wang, Z. (2021). Preparation of low temperature cure polybenzoxazine coating with enhanced thermal stability and mechanical properties by combustion synthesis approach. *Polymer*, 220, 123573. <https://doi.org/https://doi.org/10.1016/j.polymer.2021.123573>
- Pilato, L. (2010). *Phenolic Resins: A Century of Progress* (L. Pilato, Ed.). Springer-Verlag <https://doi.org/DOI: 10.1007/978-3-642-04714-5>
- Salnikov, D., Gorodisher, I., & Webb, R. J. (2014). Polybenzoxazine composition. In: WO 2014052255 A1.
- Schreiber H. (1973). *German Patent 2 255 504*.
- Shukla, S., Ghosh, A., Roy, P. K., Mitra, S., & Lochab, B. (2016). Cardanol benzoxazines – A sustainable linker for elemental sulphur based copolymers via inverse vulcanisation. *Polymer*, 99, 349-357. <https://doi.org/https://doi.org/10.1016/j.polymer.2016.07.037>
- Sudo, A., Hirayama, S., & Endo, T. (2010). Highly efficient catalysts-acetylacetonato complexes of transition metals in the 4th period for ring-opening polymerization of 1,3-benzoxazine. *Journal of Polymer Science Part A: Polymer Chemistry*, 48(2), 479-484. <https://doi.org/DOI:10.1002/pola.23810>
- Sun, J., Wei, W., Xu, Y., Qu, J., Liu, X., & Endo, T. (2015). A Curing System of Benzoxazine with Amine: Reactivity, Reaction Mechanism and Material Properties [10.1039/C4RA16582A]. *RSC Advances*, 5(25), 19048-19057. <https://doi.org/DOI: 10.1039/C4RA16582A>

10.1039/C4RA16582A

- Urbaniak, T., Soto, M., Liebeke, M., & Koschek, K. (2017). Insight into the Mechanism of Reversible Ring-Opening of 1,3-Benzoxazine with Thiols. *The Journal of Organic Chemistry*, 82(8), 4050-4055. <https://doi.org/DOI: 10.1021/acs.joc.6b02727>
- Wang, P., Liu, M., & Ran, Q. (2020). The study on curing and weight-loss mechanisms of benzoxazine during thermal curing process. *Polymer Degradation and Stability*, 179, 109279. <https://doi.org/https://doi.org/10.1016/j.polymdegradstab.2020.109279>
- Yagci, Y., Kiskan, B., & Ghosh, N. N. (2009). Recent Advancement on Polybenzoxazine-A Newly Developed High Performance Thermoset. *Journal of Polymer Science, Part A: Polymer Chemistry*, 47(21), 5565-5576. <https://doi.org/10.1002/pola.23597>
- Zakzeski, J., Bruijninx, P. C. A., Jongerius, A. L., & Weckhuysen, B. M. (2010). The Catalytic Valorization of Lignin for the Production of Renewable Chemicals. *Chemical Reviews*, 110(6), 3552-3599. <https://doi.org/10.1021/cr900354u>
- Zong, J., & Ran, Q. (2019). Ring Opening Reaction of 3,4-Dihydro-2H-1,3-Benzoxazine with Amines at Room Temperature. *ChemistrySelect*, 4(22), 6687-6696. <https://doi.org/https://doi.org/10.1002/slct.201901447>
- Zúñiga, C., Larrechi, M. S., Lligadas, G., Ronda, J. C., Galià, M., & Cádiz, V. (2011). Polybenzoxazines from renewable diphenolic acid. *Journal of Polymer Science Part A: Polymer Chemistry*, 49(5), 1219-1227. <https://doi.org/DOI: 10.1002/pola.24541>